JIPB Journal of Integrative Plant Biology

Research Article
https://doi.org/10.1111/jipb.70158

Calcium signaling mediated by glutamate receptor-like protein PagGLR3.3 is involved in tension wood induction in poplar

Yi An[1†], Mei-Qiao Qu[1†], Ya Geng[1], Xue Jiao[1], Xue-Qin Song[2], Shu-Tang Zhao[2], Xiao Han[1], Li-Chao Huang[1], Jin Zhang[1], Jie-Hua Wang[1], Suzanne Gerttula[3], Andrew Groover[3] and Meng-Zhu Lu[1*]

1. National Key Laboratory for Development and Utilization of Forest Food Resources, Zhejiang Key Laboratory of Forest Genetics and Breeding, Plant Cell Wall Research Centre, College of Forestry and Biotechnology, Zhejiang A&F University, Hangzhou 311300, China
2. State Key Laboratory of Tree Genetics and Breeding, Research Institute of Forestry, Chinese Academy of Forestry, Beijing 100091, China
3. US Forest Service, Northern Research Station, Burlington, Vermont 05405, USA
†These authors contributed equally to this work.
*Correspondence: Meng-Zhu Lu (lumz@zafu.edu.cn)

Yi An

Meng-Zhu Lu

ABSTRACT

Tension wood (TW), a type of reaction wood that develops in angiosperm trees in response to gravistimulation, serves as an ideal model for investigating the regulatory mechanisms underlying xylem cell differentiation and cell wall deposition. The initial biological signals that induce the formation of reaction wood in response to gravitational stimuli remain poorly understood. In this study, we utilized pharmacological and genetic approaches to modulate Ca^{2+} levels in hybrid white poplar (*Populus alba* × *P. glandulosa*) and examine the role of calcium signaling during the early stages of gravitropic responses. Our findings revealed differential cytosolic Ca^{2+} signal distribution in gravistimulated stems during the early phase of gravity induction, characterized by lower Ca^{2+} levels on the upper side (where TW forms) and higher Ca^{2+} levels on the lower side (where opposite wood forms). Consistent with this hypothesis, plants treated with $LaCl_3$ and those with genetically disrupted calcium channels (*PagGLR3.3* knockout using the CRISPR/Cas9 system) showed reduced Ca^{2+} signals and developed characteristic TW features. These results suggest that decreased Ca^{2+} levels induce the formation of TW. Furthermore, *PagGLR3.3* knockout plants with TW-like stems displayed diminished sensitivity to gravistimulation. Transcriptomic analysis revealed that the knockout of *PagGLR3.3* resulted in the upregulation of genes associated with TW formation and reactive oxygen species (ROS) production. Notably, superoxide anion ($O_2^{\cdot-}$) levels were significantly elevated in the cambium zone of stems subjected to gravistimulation, $LaCl_3$ treatment, or *PagGLR3.3* knockout, indicating that reduced Ca^{2+} levels promote TW formation through increased $O_2^{\cdot-}$ accumulation. This study offers novel insights into the critical role of Ca^{2+} in gravitropism and TW induction in poplar.

Keywords: Ca^{2+}, gravistimulation, $O_2^{\cdot-}$, *PagGLR3.3*, *Populus*, tension wood

An, Y., Qu, M.-Q., Geng, Y., Jiao, X., Song, X.-Q., Zhao, S.-T., Han, X., Huang, L.-C., Zhang, J., Wang, J.-H., et al. (2026). Calcium signaling mediated by glutamate receptor-like protein PagGLR3.3 is involved in tension wood induction in poplar. J. Integr. Plant Biol. **00:** 1–18.

INTRODUCTION

Wood functions as one of the most significant reservoirs of sequestered carbon within the terrestrial biosphere and represents a critical, sustainable resource for biofuels, bioenergy production, and the synthesis of refined chemicals (Richter et al., 1999; Ragauskas et al., 2006; An et al., 2021). The formation of wood is a complex, tissue-specific

development process that begins in the vascular cambium, where cells divide and differentiate into secondary xylem cells (Ye, 2002). When tree stems are subjected to displacement by factors such as wind, erosion, or other environmental influences, they develop specialized tissues known as reaction wood, which generates forces to reorient the stem (Mellerowicz and Gorshkova, 2012; Groover, 2016; Wang et al., 2017; Du et al., 2020). In angiosperm trees, tension wood (TW), a specific type of reaction wood, develops on the upper side of inclined or bent stems as a response to gravitational stimuli. The morphology, anatomy, ultrastructure, and chemical composition of TW show significant deviations from those of normal wood (NW). These deviations include an increased abundance of xylem fiber cells, a decreased presence of vessel elements, elevated cellulose content, and reduced lignin content (Wu et al., 2000; Pilate et al., 2004; Liu et al., 2021). A distinctive characteristic of TW is the presence of a gelatinous cell wall layer (G-layer), which plays a pivotal role in facilitating the stem's return to its original vertical orientation (Somerville, 2006; Gritsch et al., 2015; Groover, 2016; Zinkgraf et al., 2018).

Previous studies have demonstrated that numerous transcription factors (TFs) are involved in TW formation in *Populus*. The expression of *Arborknox2* affects TW fiber development and gravibending in *P. alba* × *P. tremula* (Gerttula et al., 2015); ethylene response factors (*ERFs*) modulate the formation of wood with TW properties; overexpression of *ERF139* decreases vessel diameter (Vahala et al., 2013), while overexpression of *ERF18* and *ERF21* increases the carbohydrate content in *P. tremula* × *P. tremuloides* (Felten and Sundberg, 2013); *Class B3 heat shock 3-1* (*HSFB3-1*) and *MYB092* regulate the expression of secondary cell wall (SCW) genes during TW formation in *P. trichocarpa* (Liu et al., 2021); *MYB128* regulates G-layer formation in fiber cells during brassinosteroid-mediated TW formation by activating the expression of cellulose synthase genes (*CesAs*) in *P. davidiana* × *P. bolleana* (Jin et al., 2020); and CRISPR-based knockout of *lateral organ boundaries domain 39/22* (*LOB39/22*) strongly inhibits TW formation, reduces the cellulose content, and increases the lignin content in *P. trichocarpa* (Yu et al., 2022b). In addition, transcriptomic studies reveal that *CesA8-2* and *CesA3-2* are highly expressed in TW compared to NW in *P. tremula* × *P. tremuloides* (Andersson-Gunneras et al., 2006). *PtrCesA1*, *PtrCesA2*, and *PtrCesA3* in *P. tremuloides*, homologous to the secondary wall-associated *CesAs* in *Arabidopsis*, influence TW formation (Bhandari et al., 2006). Plant hormones, such as auxin, ethylene, gibberellin, and brassinosteroid, play crucial roles in TW development (Gerttula et al., 2015; Wang et al., 2017; Felten et al., 2018; Du et al., 2020). Recently, our research has demonstrated that superoxide anion ($O_2^{\cdot-}$) levels markedly increase in the cambium zone on the TW-forming side of the stem within 12 h of gravistimulation, compared to the opposite wood (OW)-forming side. This elevation in $O_2^{\cdot-}$ levels subsequently promotes IAA accumulation on the TW-forming side, accelerating cambium cell proliferation and ultimately inducing TW formation (Huang et al., 2024). However, the initial signals triggered by gravitational stimulation that precede the increase in $O_2^{\cdot-}$ levels remain to be elucidated.

Plants show rapid responses to stress through both localized and systemic mechanisms, which prompt undamaged regions to initiate defensive reactions (Toyota et al., 2018). Reactive oxygen species (ROS), electrical signals, and fluctuations in cytosolic calcium ion concentration ($[Ca^{2+}]_{cyt}$) are proposed to form signaling networks that facilitate both local and systemic defense responses (Takahashi and Shinozaki, 2019). Ca^{2+} plays a pivotal role in conferring resistance to biotic and abiotic stresses (Wilkins et al., 2016; Aldon et al., 2018), providing an indispensable mechanism for sessile organisms to rapidly respond and adapt to dynamic environmental conditions by modulating their developmental programs (Luan, 2009; Dodd et al., 2010). A transient and defined pattern of $[Ca^{2+}]_{cyt}$ changes is considered a "second messenger" that is both necessary and sufficient to trigger downstream responses (Gilroy and Trewavas, 2001; Kudla et al., 2018). Various Ca^{2+} signals can be encoded as spikes, waves, and oscillations, interpreted by Ca^{2+} sensors and effectors to elicit specific cellular responses (Seybold et al., 2014). Exposure to environmental stress induces rapid local changes in cytosolic Ca^{2+} levels that are sensed and relayed within the cell, and this process activates respiratory burst oxidase homolog D (RBOHD) proteins, generating an apoplastic ROS burst (Devireddy et al., 2020). The interplay between Ca^{2+} and ROS waves, along with the electric signals, facilitates directional cell-to-cell systemic signaling and even plant-to-plant communication (Foyer and Hanke, 2022; Ravi et al., 2023). While Ca^{2+} has been shown to influence wood formation in trees (Lautner, et al., 2007), the role of Ca^{2+} signaling in the gravitropic response of trees and the formation of reaction wood remains uninvestigated. Evidence suggests that the in vivo mechanisms of ion channels from the glutamate receptor-like (GLRs) family in plants resemble those of animal iGluRs, prompting speculation that GLRs may encode plant Ca^{2+}-permeable nonselective cation channels mediating the influx of Na^+, K^+, and Ca^{2+} into cells (Lam et al., 1998; Meyerhoff et al., 2005; Wudick et al., 2018). Previous studies have shown that GLRs are involved in plant root gravitropism and defense signaling (Miller et al., 2010). Specifically, GLR3.3 functions as an essential calcium channel protein in plants (Nguyen et al., 2018; Toyota et al., 2018; Yan et al., 2024). Although GLRs serve as channels that convert stimulus signals into increased intracellular Ca^{2+} concentrations, which propagate to distal organs and thereby triggering defense responses (Mousavi et al., 2013; Toyota et al., 2018; Yu et al., 2022a), the involvement of GLRs in normal growth and gravity response in woody plants remains elusive.

In this study, we examined the role of Ca^{2+} signaling in the early induction of TW formation through pharmacological and genetic manipulation of Ca^{2+} levels in white poplar 84 K (*P. alba* × *P. glandulosa*). Gravity-induced stimulation and transcriptomic analysis revealed that *PagGLR3.3* mediates a

decrease in Ca^{2+} levels on the TW-forming side of gravistimulated stems, resulting in increased $O_2^{\cdot-}$ accumulation and subsequent TW induction. These findings provide novel insights into the regulatory mechanisms of Ca^{2+} in wood formation.

RESULTS

Ca^{2+} distribution was altered in phloem cells in response to gravistimulation

One-month-old 84 K poplar plants grown in soil were subjected to horizontal positioning for gravistimulation. Within 2 h, the shoot tips showed a slight upward curvature, and by 4 h, they had nearly resumed an upright orientation (Figure 1A), indicating an early response to gravistimulation during this period. We collected samples from the middle segment of the stem between the base and the bent apex (primary bending region), where the TW was intensively formed in the later stage (secondary bending). To investigate whether Ca^{2+} levels altered in the initial response to gravistimulation, we utilized three distinct methodologies for *in situ* Ca^{2+} localization, given the challenges associated with real-time imaging of vascular tissues. To minimize potential alterations in Ca^{2+} levels caused by the wounding response during sampling, stems were promptly segmented and immediately submerged in a fixative solution. The calcium antimoniate precipitate method was performed by adding antimonite in fixative solution and the antimonite calcium deposits were observed under transmission electron microscopy (TEM). Results indicated that Ca^{2+} primarily accumulated in phloem parenchyma cells (PPCs) adjacent to the cambium, while minimal Ca^{2+} was detected in the cambium and developing xylem (Figure S1A). Energy-dispersive X-ray microanalysis (EDX) and Ca^{2+}-sensitive fluorescent dye (CaFD) staining of cross sections similarly revealed that Ca^{2+} was predominantly concentrated in PPCs (Figure S1B, C). Consistent results across all three methods suggest their reliability in detecting Ca^{2+} distribution.

During gravistimulation, the distribution of Ca^{2+} in PPCs showed no difference between the upper side (TW-forming) and the lower side of the stem at the onset of gravistimulation (0 h), as revealed by EDX and CaFD staining (Figures S2, S3). However, from 1.5 to 3.5 h, a marked reduction in Ca^{2+} concentration was observed on the upper side, while a corresponding increase occurred on the lower side. Notably, the disparity in Ca^{2+} concentration peaked at 2 h. By 4 h, Ca^{2+} levels began to re-equilibrate. TEM observations of 84 K stems subjected to gravistimulation at 0, 2, and 4 h further confirmed that the TW-forming side showed a lower Ca^{2+} concentration during the early stages of gravity induction (within 2 h) (Figure 1B, C). These findings suggest that fluctuations in Ca^{2+} may play a crucial role in the initial response to gravistimulation.

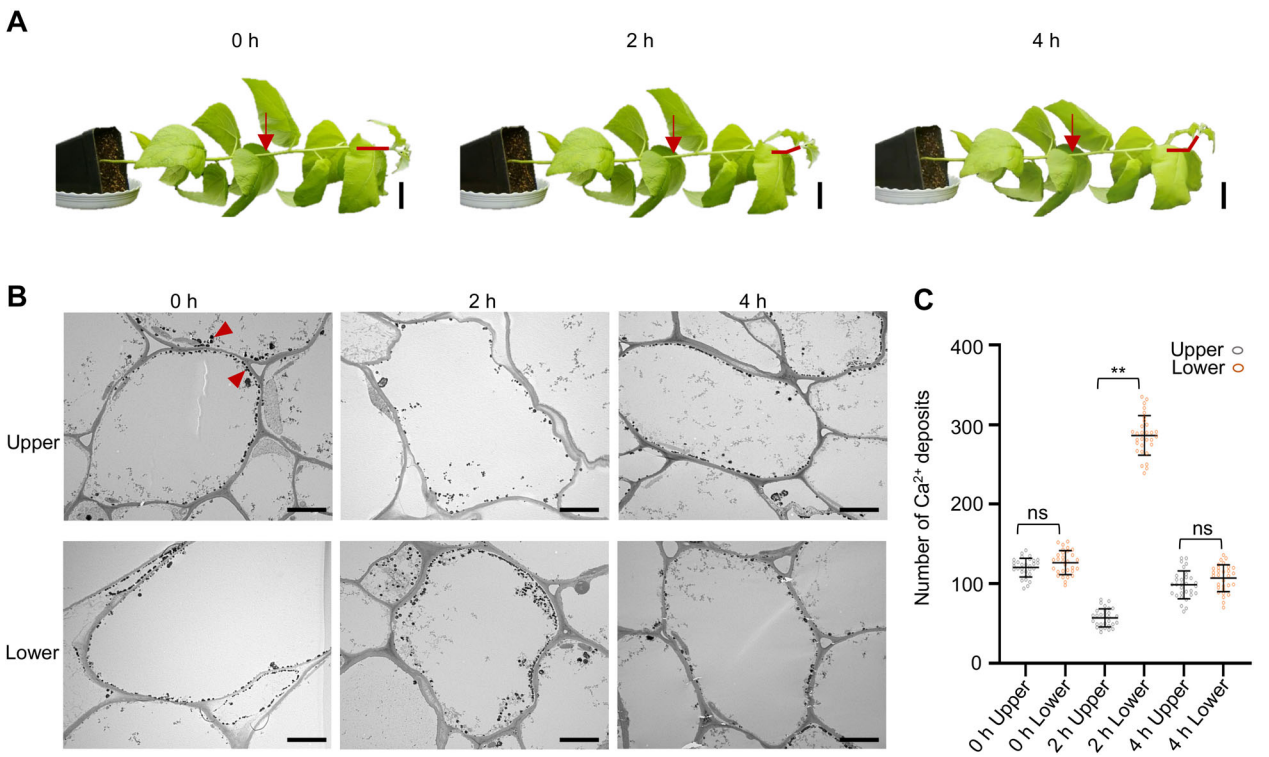

Figure 1. Distribution of Ca^{2+} in phloem parenchymal cells (PPCs) of 84 K plants during early gravistimulation

(A) Apex subjected to gravistimulation for 0 h, 2 h, and 4 h. The red line indicates the stem region of the apex. The red arrow indicates the sampling site for Ca^{2+} observation in **(B)**, located midway along the stem between the base and the bent apex. Bars = 5 cm. **(B)** TEM images showing Ca^{2+} deposits. Red arrows highlight representative Ca^{2+} deposits. Bar = 5 μm. **(C)** Quantitative analysis of Ca^{2+} deposits in PPCs on the upper and lower sides of the stem. Thirty images were randomly selected and analyzed, with the Ca^{2+} deposits counted per unit area (50 × 50 μm) using ImageJ software.

Reduced Ca^{2+} levels led to TW formation

To investigate the impact of altered Ca^{2+} distribution on the gravitropic response of poplars, we applied lanthanum chloride ($LaCl_3$), a calcium channel inhibitor, to 1-month-old soil-grown plants at concentrations of 100 mM, 200 mM, and 300 mM for 14 d. The stem curvature in $LaCl_3$-treated plants was significantly reduced compared to that of untreated controls. Moreover, the degree of stem curvature showed an inverse relationship with the concentration of $LaCl_3$ applied (Figure S4A, B). To rule out the potential influence of Cl^-, we conducted additional experiments using $CaCl_2$ (450 mM) and KCl (900 mM), ensuring equivalent Cl^- concentrations for gravity induction. The results indicated no significant differences in stem curvature among the $CaCl_2$, KCl, and control groups (Figure S4C, D). These findings further substantiate that gravitropism-induced stem curvature is modulated by Ca^{2+} levels.

To investigate the impact of altered Ca^{2+} distribution on wood development, 1-month-old soil-grown plants were treated with $LaCl_3$ (300 mM) for 14 d. Compared to control plants, $LaCl_3$-treated plants showed reduced height growth (Figure 2A), but enhanced radial expansion with increased xylem width, as evidenced by cross sections of the 10th internodes (Figure 2B, C). Histological staining using Astra blue revealed the presence of G-layers, a characteristic feature of TW, in $LaCl_3$-treated plants, whereas such layers were absent in untreated controls (Figure 2B, D). These findings suggest that inhibition of Ca^{2+} influx or a low cytosolic Ca^{2+} concentration may trigger the formation of tension wood.

PagGLR3.3 knockout plants presented altered wood property

GLR3.3 are important calcium channels in plants. We previously showed that *PagGLR3.3b* expression was significantly upregulated in poplar stems under conditions of Ca^{2+} deficiency (An et al., 2024). Through phylogenetic analysis, we identified two homologous genes of *AtGLR3.3*, *PagGLR3.3a*, and *PagGLR3.3b*, which were predominantly expressed in the phloem, as evidenced by GUS staining of the stem in transgenic plants driven by their respective promoters (An et al., 2024). To investigate the potential functions of *PagGLR3.3*, we utilized poplar lines in which both genes were knocked out (An et al., 2024). To investigate the role of PagGLR3.3 in Ca^{2+} flux, we measured the Ca^{2+} fluxes in the roots of *crispr-PagGLR3.3* plants using non-invasive micro-test technology (NMT). The results indicated that the #3, #6, and #9 *crispr-PagGLR3.3* lines showed 76.3%, 72.9%, and 76.1% lower influx compared to the control plants, respectively (Figure S5), indicating that PagGLR3.3 functions as an important Ca^{2+} channel.

Similar to the $LaCl_3$-treated plants, the *PagGLR3.3* knockout plants grew more slowly in height (Figure 3A), but presented faster radial growth and greater stem diameter than the wild-type controls (Figure 3B, C). The anatomical phenotypes of the three *crispr-PagGLR3.3* lines were consistent. Then, we chose line 9 for further data analysis. Compared with the controls, *crispr-PagGLR3.3#9* increased approximately 93%, 25%, and 25% in xylem, cambium, and cortex widths, respectively, as quantified on the stem

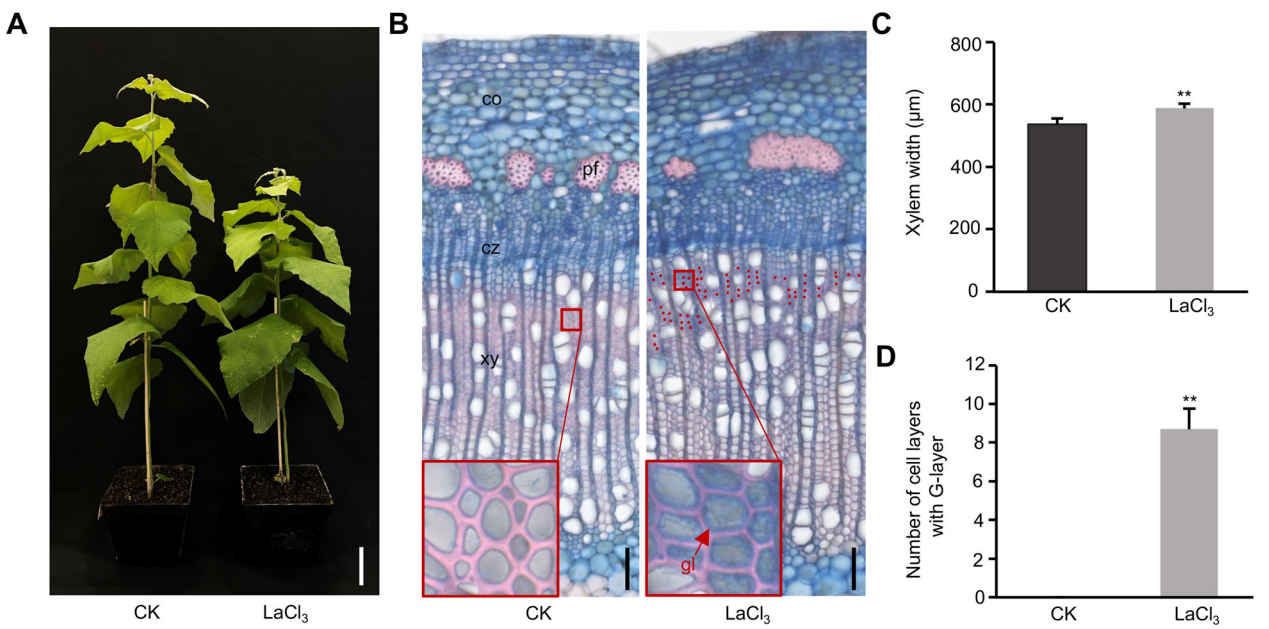

Figure 2. "Tension wood" formation in upright 84 K plants under $LaCl_3$ treatment

(A) Phenotypic comparison between $LaCl_3$-treated ($LaCl_3$) and untreated 84 K plants (CK). Bars = 5 cm. **(B)** Histological staining of cross-sections of the 10th internodes of upright plants with safranin and Astra blue. Red dots denote cells containing a G-layer, while the arrow indicates the position of the G-layer (gl) in the cell in the magnified image (enlarged image inserted). co, cortex; cz, cambium zone; pf, phloem fiber; xy, xylem. Bars = 100 μm. **(C, D)** Statistical analysis of the xylem width **(C)** and the number of xylem cell layers showing a G-layer **(D)** in the 10th internodes of upright stems.

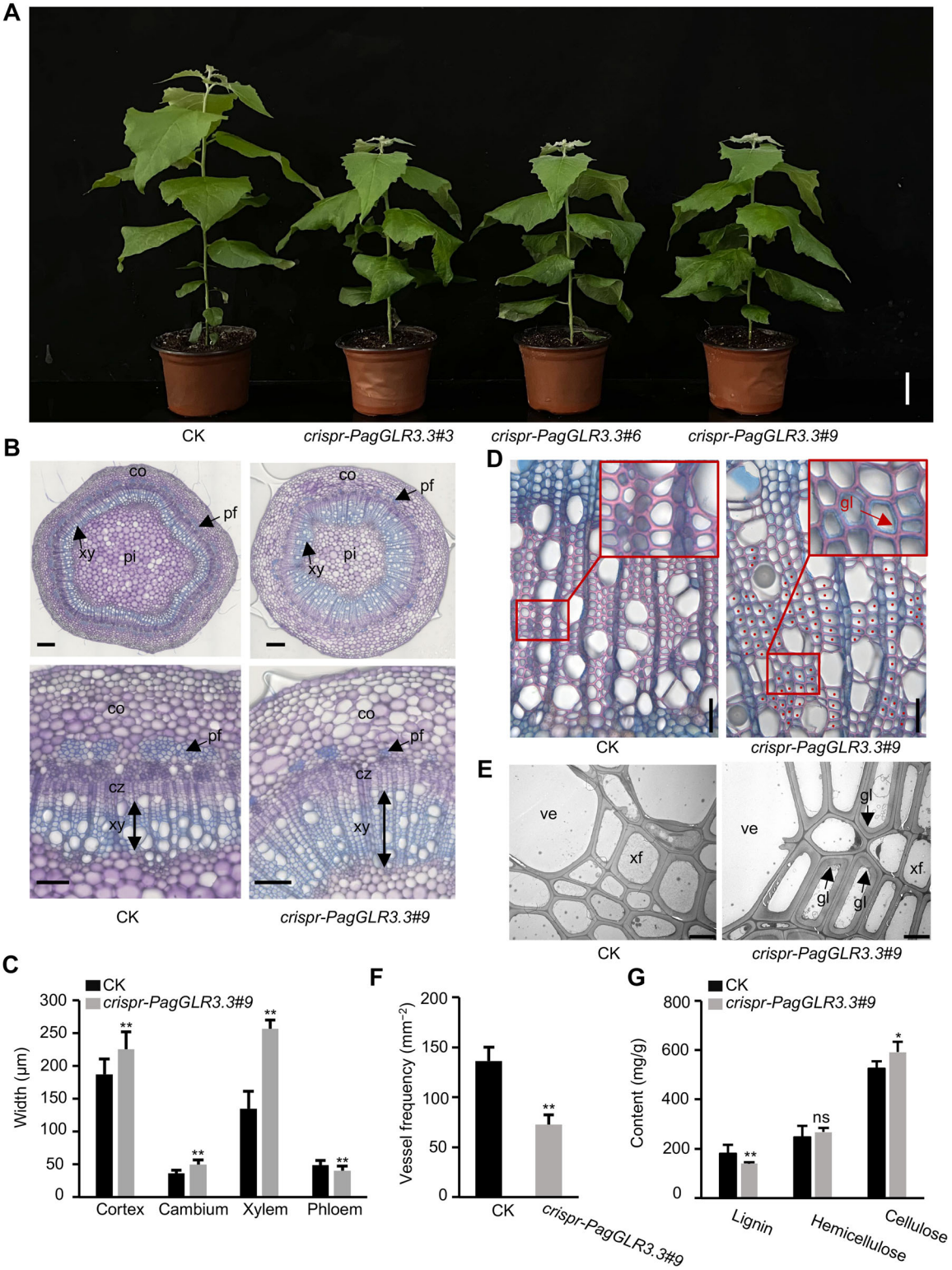

Figure 3. Phenotypic analyses of *crispr-PagGLR3.3* plants

(A) Plants under normal growth conditions. Bars = 5 cm. **(B)** Stem cross-sections of the seventh internodes with TBO staining. Bars = 100 μm. **(C)** Measurement of the cortex, cambium, xylem, and phloem widths. **(D)** Cross-sections of the seventh internodes of upright plants stained with safranin and Astra blue. Red dots indicate cells containing a G-layer, and the arrow points to the position of the typical G-layer (gl) within the cell (inserted enlarged image). Bars = 50 μm. **(E)** TEM images showing the ultrastructure of xylem cells, highlighting the presence of the G-layer (gl). Arrows indicate the position of the G-layer (gl) in the cell. **(F)** Vessel frequency (per mm^{-2}) in cross-sections of the seventh internodes of upright plants. **(G)** Quantification of lignin, hemicellulose, and cellulose content in the stems. co, cortical; cz, cambium zone; pf, phloem fiber; ve, vessel, xy, xylem.

sections of the seventh internodes, though the phloem width decreased by 20% (Figure 3B, C). Interestingly, the upright *crispr-PagGLR3.3#9* plants had G-layers (Figure 3D), as shown using Astra blue staining, and were further confirmed by the presence of G-layers in both xylem and phloem fiber cells in *crispr-PagGLR3.3#9* plants using STM (Figures 3E, S6). In contrast, there were no G-layers in these cells in the upright non-transgenic controls (Figure 3D, E). We also generated overexpression lines (*OEPagGLR3.3a* and *OEPagGLR3.3b*); no G-layer was observed in the upright stems (Figure S7). In addition, *crispr-PagGLR3.3#9* plants presented lower numbers of vessel cells (Figure 3F), another typical TW feature, compared to non-transgenic controls. Furthermore, higher cellulose content was revealed by calcofluor white staining (Figure S8A), while lower lignin was revealed by phloroglucinol–HCl staining (Figure S8B) of the secondary walls of *crispr-PagGLR3.3#9* plants than those of the control plants. By quantification, the cellulose content in *crispr-PagGLR3.3#9* plants increased by 13%, whereas the lignin content decreased by 22%, compared to that in the control plants (Figure 3G). These results demonstrated that the wood formed in *crispr-PagGLR3.3* plants has a typical TW property, indicating that *PagGLR3.3* is involved in the regulation of TW formation.

PagGLR3.3 affected TW formation in response to gravistimulation

We investigated the gravitropic response of 1-month-old soil-grown *crispr-PagGLR3.3#9* plants by analyzing time-lapse video recordings over a 20-d period (Movie S1). At the onset of gravistimulation, the rate of primary bending in the elongating shoot tips of *crispr-PagGLR3.3#9* plants was significantly reduced compared to that of the control plants (Movie S2). Specifically, the shoot tips of control plants initiated upward movement within 2 h post-gravistimulation and reached an almost vertical orientation within 4 h (Figure 4A). In contrast, the shoot tips of *crispr-PagGLR3.3#9* plants showed minimal changes within the first 2 h following gravistimulation and only showed a slight upward after 4 h. Ultimately, it took approximately 10 h for the shoot tips to achieve a mostly upright position and 15 h to fully recover to a vertical orientation (Figure 4A). These observations suggest that *crispr-PagGLR3.3* plants show a delayed primary bending response to gravistimulation relative to control plants. Secondary bending of the lower stem in control plants occurred 4.5 d after gravistimulation, whereas in *crispr-PagGLR3.3#9* plants, this phenomenon was observed at 20 d post-gravistimulation (Figure 4A). At 14 d, the extent of stem lifting and curvature was reduced by 72% and 84%, respectively, compared to control plants (Figure 4B, C). TW development is characterized by the asymmetric growth of xylem tissue, quantified by the TW/OW ratio, which is the ratio of the radial width of newly formed TW to that of opposite wood (OW) (Love et al., 2009; Felten et al., 2018; Yu et al., 2022b). A higher TW/OW ratio indicates more intensive TW development (Yu et al., 2022b). We sectioned the stems midway between the base and the apex bend, where TW formation is most pronounced in later stages, and found that the TW area width and the TW/OW ratio were reduced by 45% and 20%, respectively, in *crispr-PagGLR3.3#9* plants compared to controls (Figure 4D–F). Gravity-induced stimulation assays revealed that *OEPagGLR3.3* plants showed a significantly earlier response than the control in primary bending (Movie S3). These results confirm an association between TW formation and reduced Ca^{2+} levels.

To elucidate the underlying cause of the attenuated gravity response in *crispr-PagGLR3.3* plants, we conducted Astra blue staining and observed that G-layers were present in both TW and OW in *crispr-PagGLR3.3#9* plants, whereas they were only detected in TW in control plants (Figure 4G). We further confirmed these findings through immunolocalization studies using monoclonal antibodies JIM14 for arabinogalactan protein (AGP) and LM5 for (1–4)-β-galactan (Figure S9). Consistent with previous reports (Arend, 2008; Gritsch et al., 2015; Xu et al., 2021), (1–4)-β-galactan was exclusively localized in TW fibers. Interestingly, similar results were observed in the $LaCl_3$-treated plants under gravistimulation. The mock-treated controls showed a significant increase in gravibending stem lift and curvature, whereas the $LaCl_3$-treated plants demonstrated a delayed response (Figure S10A–C). Consequently, $LaCl_3$-treated plants showed a reduced radial width of TW by 45%, while the radial width of OW remained similar to that of the controls (Figure S10D, E), resulting in a decreased TW/OW radial width ratio in $LaCl_3$-treated plants (Figure S10F). Additionally, the $LaCl_3$-treated plants displayed a G-layer in the OW, which was absent in the controls (Figure S10D). These findings suggest that the preformed TW in both *crispr-PagGLR3.3* and $LaCl_3$-treated plants may also exert a "pulling force" by G-layer on the OW side of the stems, thereby delaying the gravity responses in these plants.

To further investigate whether the preformed G-layers influence the gravibending response in plants, 1-month-old 84 K plants grown in soil were subjected to 2 weeks of continuous gravistimulation to induce G-layer formation (Figure S11A, B). Subsequently, these plants were rotated 180° with the shoot tip positioned downward (Figure S11C). After an additional week, the shoot tips of the rotated plants showed a horizontal looping growth pattern, followed by upward growth, while the stem bodies remained unchanged (Figure S11D). In contrast, control plants that were not subjected to rotation maintained their upward growth and showed robust development over the 3-week gravistimulation period (Figure S11E). Cross-sectional analysis of the 10th and 15th internodes revealed differences in the thickness of TW between control and rotated plants. In control plants, TW was predominantly localized on one side of the stem, whereas in rotated plants, TW formation was reduced bilaterally (Figure S11F). The presence of G-layers in OW may attenuate the plant's response to gravity, leading to a delayed recovery of stem orientation. Consequently, G-layers may impede the gravibending response in *crispr-PagGLR3.3* plants.

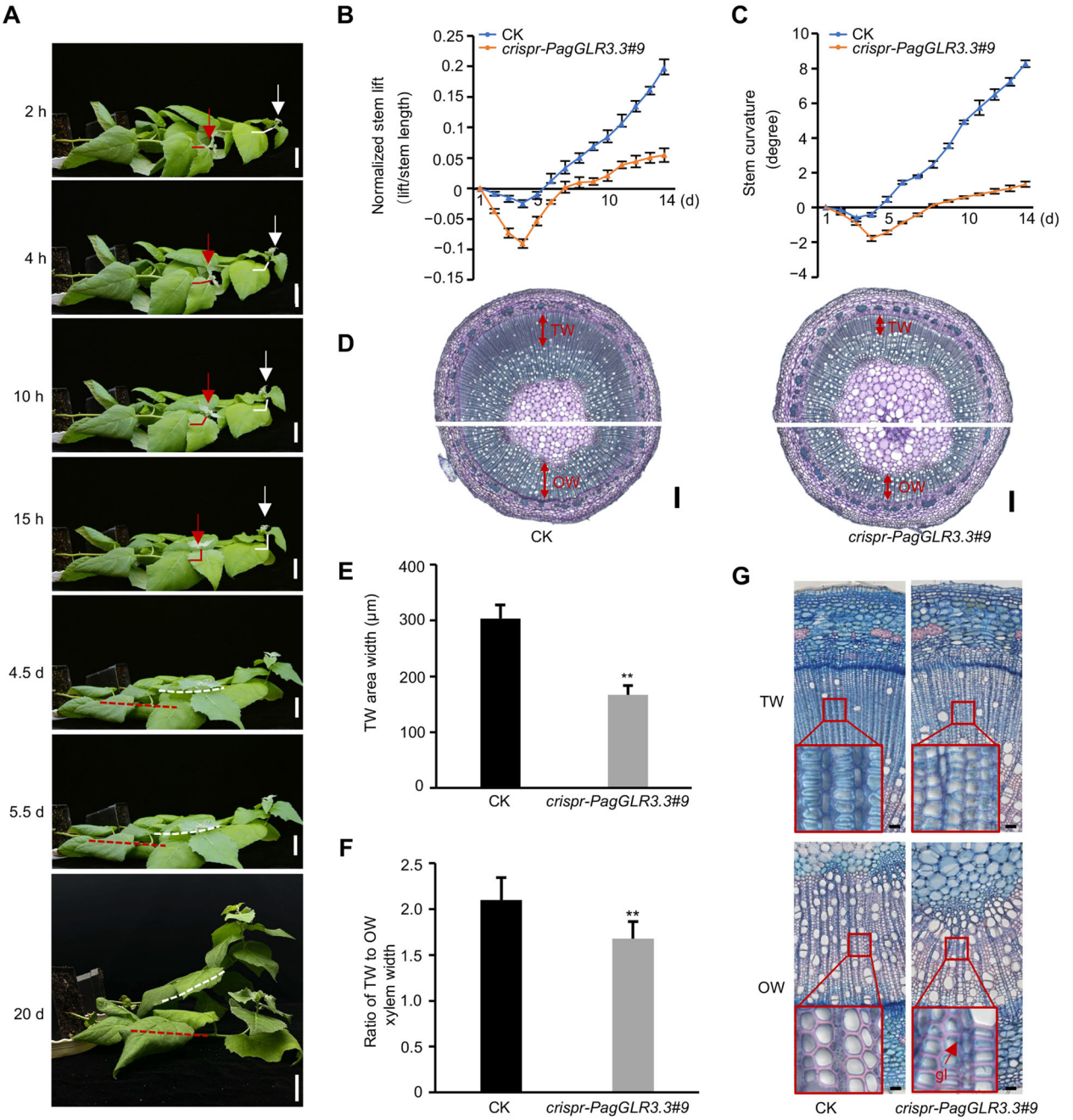

Figure 4. *PagGLR3.3* knockout resulted in delayed tension wood (TW) formation

(A) Divergent responses of the apex (arrows) and the stem (dashed lines) of CK (white) and *crispr-PagGLR3.3#9* (red) plants to gravistimulation. Bars = 5 cm. **(B)** Graph depicting the apex curvature represented as the ratio of the height of the tip to the length of the stem over time. **(C)** Graph depicting the changes in stem curvature represented as the angle between the lifted stem and the horizontal line over time. **(D)** Transverse sections from stems subjected to 14 d of gravistimulation stained with TBO. The sample site was in the middle of the stem between the base and the bent point of the apex. Bars = 200 μm. **(E)** Quantification of TW area width. **(F)** Statistical analyses of the ratio of TW to OW xylem width. **(G)** Cross sections of TW and OW safranin and Astra blue staining for the G-layer. The arrow indicates the position of the G-layer (gl) within the cells (enlarged image inserted).

crispr-PagGLR3.3 plants with retarded Ca^{2+} flux attenuated the response to gravistimulation

To investigate whether Ca^{2+} flux is channeled through PagGLR3.3, we analyzed Ca^{2+} distribution during TW induction using calcium antimoniate precipitates: EDX and CaFD. The results showed that *crispr-PagGLR3.3#9* plants had altered distribution of Ca^{2+} in PPCs (Figure 5). In upright plants (before gravistimulation), *crispr-PagGLR3.3#9* plants showed reduced Ca^{2+} accumulation in PPCs compared to control plants. Following 2 h of gravistimulation, Ca^{2+} accumulation decreased on the upper side but increased on the lower side of the stems in control plants (Figure 5), coinciding with the lifting of their shoot tips (Figure 4A). In contrast, there was minimal change in Ca^{2+} distribution in *crispr-PagGLR3.3#9* plants. After

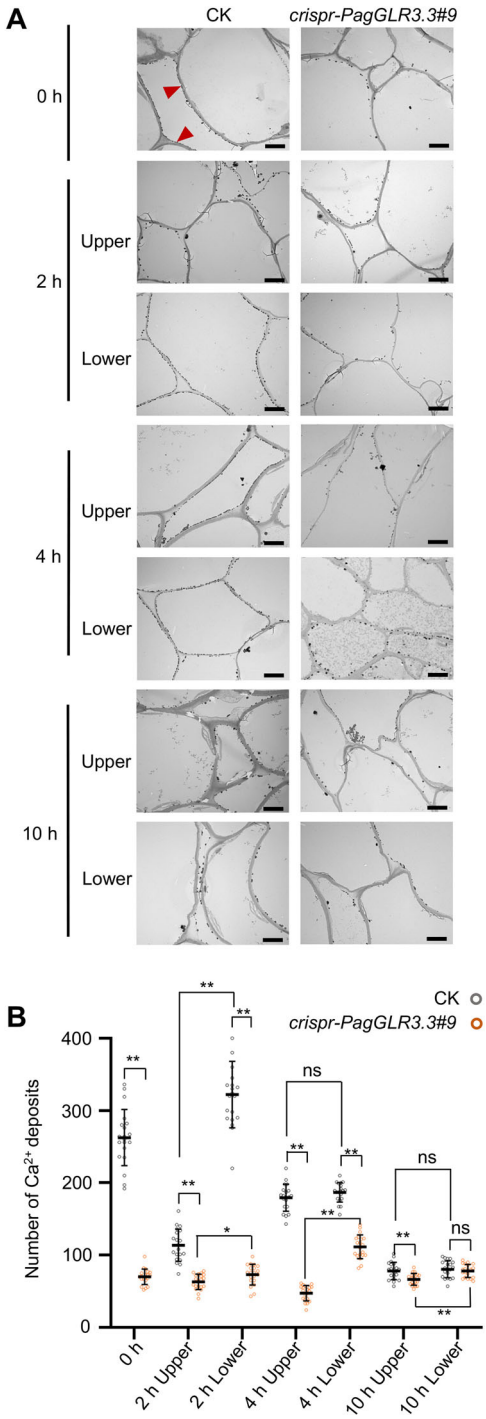

Figure 5. Accumulation of Ca^{2+} in the phloem parenchyma cells (PPCs) of CK and *crispr-PagGLR3.3#9* plants under gravistimulation
(A) Distribution of Ca^{2+} deposits in the upper and lower sides of the stem at 0 h, 2 h, 4 h, and 10 h post-gravistimulation. Red arrows indicate typical Ca^{2+} deposits. Bars = 5 μm. **(B)** The graph shows the temporal changes in Ca^{2+} levels during gravistimulation in **(A)**. Twenty PPC images were randomly selected, and the number of Ca^{2+} deposits was quantified as previously described.

4 h of gravistimulation, while Ca^{2+} levels between the upper and lower sides of the stem did not differ significantly in controls, a significant decrease in Ca^{2+} accumulation was observed on the upper side of *crispr-PagGLR3.3#9* plants when their shoot tips began to lift (Figure 4A), although overall Ca^{2+} levels remained low on both sides of the stem (Figure 5). Finally, after 10 h, the shoot tips of *crispr-PagGLR3.3#9* plants were mostly oriented upward (Figure 4A), and the difference in Ca^{2+} levels between the two sides was markedly reduced (Figure 5). Measurement of the relative Ca^{2+} concentrations in the PPCs of the control and *crispr-PagGLR3.3#9* plants subjected to gravistimulation by EDX and CaFD showed a similar scenario (Figures S12, S13). As expected, the dynamic Ca^{2+} distribution in poplar plants treated with $LaCl_3$ mirrored that observed in the *crispr-PagGLR3.3#9* plants under gravistimulation (Figure S14). Collectively, these findings indicate that alterations in the Ca^{2+} levels and Ca^{2+} distributions play a crucial role in the gravity response by facilitating the induction of TW formation.

Gene expressions were changed in *PagGLR3.3* knockout plants

To further explore the regulatory mechanism underlying TW formation involving *PagGLR3.3*, we performed a comprehensive transcriptomic analysis of stem samples from both control and *crispr-PagGLR3.3#9* plants at different developmental time points (0, 2, 4, and 10 h) post-gravistimulation. Whole-stem segments were collected at 0 h, while separate samples of the upper and down sides tissues of the segments were obtained at 2, 4, and 10 h for RNA-seq analysis. A total of 31,382 genes (90.4% of all 34,699 protein-coding genes in *Populus*) were detected across the 42 collected samples (Dataset S1). Principal component analysis indicated distinct time-specific expression patterns among the samples (Figure S15). Weighted gene co-expression network analysis (WGCNA) clustered the expressed genes into 15 modules based on their expression profiles, with module sizes ranging from 210 to 16,896 (Figure S16). Subsequently, Gene Ontology (GO) analysis was performed to assess functional enrichment within these modules. The results demonstrated that genes in the cyan module were enriched in cell cycle processes, those in the green and salmon modules were associated with cell wall biosynthesis, genes in the light green module were involved in xylem and phloem development, and genes in the purple module were related to ROS processes (Figure S17; Dataset S2). At the initial time point (0 h), representative genes highly expressed in *crispr-PagGLR3.3#9* plants included the cellulose synthase genes *CesA1*, *CesA3*, *CesA4,* *CesA7*, *CesA8*, and *CesA9*; the Fascilin-like arabinogalactian protein genes *FLA7*, *FLA9*, and *FLA12* (involved in cell wall biosynthesis); phloem intercalated with xylem (*PXY*) (vascular tissue development); and a member of the xyloglucan endotransglucosylase/hydrolase (*XTH9*) family, WUSCHEL-related homeobox 4 (*WOX4*) (cambium activity) (Figure 6A). During gravistimulation, the expression of these genes showed a similar trend, first decreasing and then increasing in both *crispr-PagGLR3.3#9* and control plants, but the changes were more rapid in control plants. After 10 h, genes such as *FLA7*, *FLA11*, and *FLA12* still showed higher expression levels in the upper side of the stem in control plants compared to

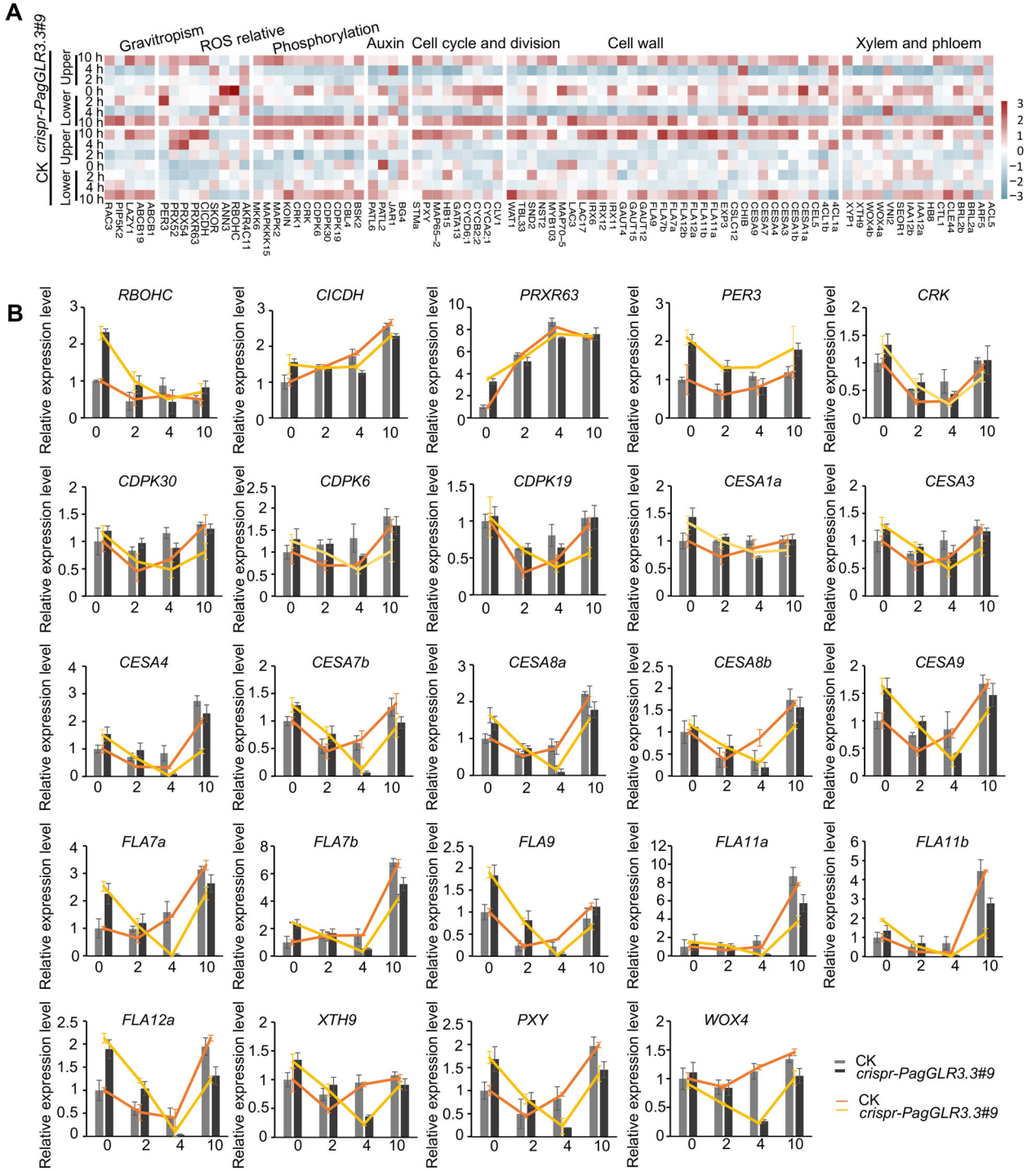

Figure 6. Transcriptomic analysis of gene expression differences between the control and *crispr-PagGLR3.3* plants during gravistimulation induction

(A) Heatmap depicting the expression patterns of differentially expressed genes related to cell cycle, cell wall, and phosphorylation processes. **(B)** Expression profiles of related genes in the upper portion of the stem. The bar chart illustrates the relative expression levels derived from RNA-seq data, while the line graph presents qRT-PCR results.

crispr-PagGLR3.3#9 plants (Figure 6B). These genes may be involved in the G-layer (rich in cellulose) formation and thus lift the stem faster in the control plants. Additionally, several phosphorylation-related genes, including calcium-dependent protein kinase (*CDPK6*, *CDPK19*, and *CDPK30*) and CDPK-related kinases (*CRKs*), displayed similar expression patterns. These genes may contribute to the observed differences in response kinetics to gravistimulation between the control and *crispr-PagGLR3.3#9* plants. Furthermore, at 0 h, some ROS-related genes in the *crispr-PagGLR3.3#9* plants were markedly

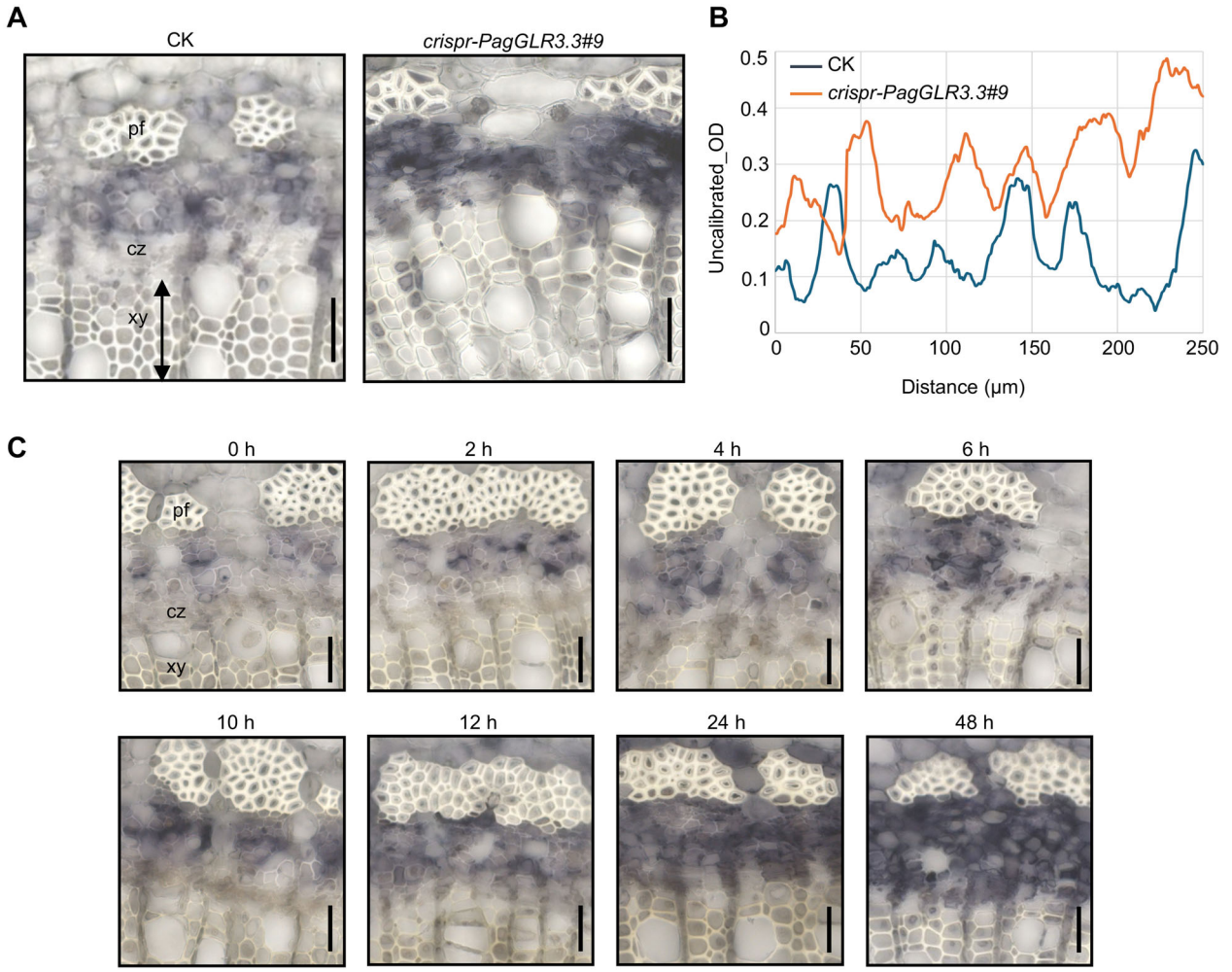

Figure 7. $O_2^{\cdot-}$ accumulation in *crispr-PagGLR3.3* and $LaCl_3$-treated plants
(A) NBT staining of seventh internode cross-sections from control and *crispr-PagGLR3.3#9* upright plants. Bars = 50 μm. **(B)** Graph depicting the intensity profiles measured over a 250 μm distance along the cambium zone. **(C)** NBT staining of seventh internode cross-sections from $LaCl_3$-treated plants at different time points throughout the treatment period. cz, cambium zone; pf, phloem fiber; xy, xylem. Bars = 50 μm.

upregulated compared to the controls (Figure 6A). These include respiratory burst oxidase protein C (*RBOHC*), cytosolic $NADP^+$-dependent isocitrate dehydrogenase (*CICDH*), and peroxidase superfamily protein (*PRXP63*, *PER3*). This indicates that fluctuations in Ca^{2+} levels can influence ROS levels within plant stems. Interestingly, our recent research has demonstrated that alterations in ROS are implicated in the induction of TW formation (Huang et al., 2024).

Reduced Ca^{2+} levels resulted in the accumulation of $O_2^{\cdot-}$ in the cambium zone

The elevated expression of ROS-related genes in *crispr-PagGLR3.3#9* plants prompted an investigation into the impact of altered Ca^{2+} distribution on ROS, particularly in $O_2^{\cdot-}$ levels. Nitroblue Tetrazolium (NBT) staining of seventh internode sections from both control and *crispr-PagGLR3.3#9* upright plants revealed that the cambium zone of *crispr-PagGLR3.3#9* plants showed significantly higher $O_2^{\cdot-}$ production compared to the control (Figure 7A, B). Similarly, $LaCl_3$-treated upright plants showed increased $O_2^{\cdot-}$ accumulation in the cambium zone, which was maintained at a high level following the prolonged treatment (Figure 7C). These results indicate that reduced Ca^{2+} levels promote $O_2^{\cdot-}$ accumulation in the cambium zone.

DISCUSSION

TW is a specialized xylem tissue formed in angiosperm trees under gravitational stimuli or mechanical stresses. Its formation in *Populus* serves as a model for studying the regulation of wood formation (Gerttula et al., 2015). Previous studies have elucidated the transcriptional and hormonal regulation of TW formation in response to gravitropism (Mellerowicz and Gorshkova, 2012; Gerttula et al., 2015; Gao et al., 2021; Yu et al., 2022b). In our recent research, we demonstrated increased $O_2^{\cdot-}$ accumulation, which occurs at 12 h post-gravistimulation in the cambium zone of the upper side of the stem to induce TW formation (Huang et al., 2024). However, the upstream mechanisms responsible for triggering

ROS signals remain unclear. In this study, we pharmacologically and genetically manipulated Ca^{2+} levels in the cytosol of poplar to investigate the role of Ca^{2+} signaling in the early gravitropic response. We observed changes in Ca^{2+} levels between the upper and lower sides of the poplar stem at 2 h post-gravistimulation, and the reduced Ca^{2+} level induced TW formation by subsequently enhancing $O_2^{\cdot-}$ accumulation. This study provides novel insights into the initial Ca^{2+} signals in gravitational stimulation-induced TW formation.

Ca^{2+} affects TW formation

As an intracellular second messenger, Ca^{2+} signaling can be triggered by gravistimulation and subsequently participates in the regulation of plant development and growth. Gravistimulation not only induces an increase in the Ca^{2+} concentration but also accelerates the occurrence of Ca^{2+} sparks (Björkman and Cleland, 1991; Monshausen et al., 2011; Zhao et al., 2022). These findings suggest that Ca^{2+} serves as a critical signal transmitter in response to gravity. Previous studies have demonstrated that xylem vessel cell differentiation is dependent on Ca^{2+}, as calcium-channel blockers significantly inhibit tracheary element differentiation (Roberts and Haigler, 1990; Kobayashi and Fukuda, 1994; Iakimova and Woltering, 2017). Additionally, poplar plants grown under calcium-deficient conditions fail to respond to environmental stimuli such as cold shock or wounding (Lautner and Fromm, 2010). However, whether Ca^{2+} is involved in gravistimulation-induced TW formation remains unclear. In this study, upright plants treated with the Ca^{2+} competitor $LaCl_3$ showed G-layer formation (Figure 2), the typical characteristic of TW. $LaCl_3$-treated plants also displayed a diminished response to gravity (Figure S10). These results indicate that Ca^{2+} levels play a pivotal role in regulating TW formation. To further explore this, we examined Ca^{2+} distribution in vascular tissues using three distinct methods (TEM, EDX, and CaFD) and found that Ca^{2+} was predominantly localized in PPCs, consistent with previous observations (Fromm, 2010). Notably, approximately 2 h after gravistimulation, we observed a significant difference in the Ca^{2+} distribution in PPCs between the upper and lower sides of the stems, with a marked reduction on the upper side of the gravistimulated stem. This suggests that the reduced Ca^{2+} level on the upper side contributes to TW formation.

Previous studies have demonstrated that changes in intracellular Ca^{2+} concentration function as a signaling mechanism for the propagation of Ca^{2+} to distal cells (Mousavi et al., 2013; Toyota et al., 2018; Yu et al., 2022a). Therefore, the mechanism by which Ca^{2+} is transported from PPCs to adjacent cambial cells warrants further investigation. GLRs are important calcium channels and extracellular amino acid sensors (Price et al., 2013), contributing to plant adaptation under biotic and abiotic stress conditions (Cheng et al., 2018; Shao et al., 2020). Consequently, the role of Ca^{2+} in gravity responses can be elucidated through the modulation of GLR channel activity. Notably, several studies have highlighted that GLR3.3 serves as an essential calcium channel protein in plants, facilitating long-distance transmission of $[Ca^{2+}]_{cyt}$ changes (Toyota et al., 2018; Yan et al., 2024). In our study, the typical characteristics of TW were observed in the upright stems of *PagGLR3.3* knockout plants, including a reduced number of vessel cells, increased cellulose content but decreased lignin content, and the presence of G-layers in both xylem and phloem fiber cells. The *crispr-PagGLR3.3* plants showed reduced Ca^{2+} accumulation in PPCs compared to control plants. Under gravistimulation, the stem bending rate of *crispr-PagGLR3.3* plants was significantly slower than that of the control group. At 2 h post-gravistimulation, Ca^{2+} accumulation decreased on the upper side but increased on the lower side of the stems in non-transgenic controls, resulting in the elevation of shoot tips. In contrast, no significant difference in Ca^{2+} levels was detected between the upper and lower sides of the stems in *crispr-PagGLR3.3* plants, causing their shoot tips to remain largely unaltered. At 4 h, Ca^{2+} accumulation decreased on the upper side but increased on the lower side of the stems in *crispr-PagGLR3.3* plants, initiating the elevation of their shoot tips. Conversely, the shoot tips of control plants were predominantly oriented upward, with a markedly reduced difference in Ca^{2+} levels between the two sides (Figures 4A, 5). We also created overexpression plants (*OEPagGLR3.3a* and *OEPagGLR3.3b*), and no G-layer was observed in the *OEPagGLR3.3* plants (Figure S7). Gravity-induced experiments showed that *OEPagGLR3.3* plants responded significantly earlier than the control in primary bending (Movie S3). These findings confirm that TW formation is associated with low Ca^{2+} levels. Therefore, this study bridges the gap between the initial signal and TW formation, offering novel insights into the role of Ca^{2+} in xylem cell differentiation.

Blocking of Ca^{2+} flow causes the G-layer formation

A typical feature of TW is the formation of the G-layer, which facilitates fibril contraction during maturation and functions as a "muscle-like tissue" to meet various mechanical demands, such as adjusting the orientation of plant axes (Gorshkova et al., 2018). In our study, both $LaCl_3$-treated upright plants and *PagGLR3.3* knockout upright plants showed G-layers in developing wood without gravistimulation (Figures 2, 3), suggesting that G-layer formation may be attributed to reduced Ca^{2+} levels. Additionally, *crispr-PagGLR3.3* plants showed much slower lifting of their stems than control plants due to the presence of "muscle-like tissue" throughout their stems prior to gravistimulation. The experiment involving a 180° rotation of 84 K plants with preformed TW (Figure S11) further corroborates this conclusion. The G-layers are rich in cellulose (Nishikubo et al., 2007), and *crispr-PagGLR3.3* plants indeed show G-layers with high cellulose content under normal growth conditions (Figure 3). Transcriptome data analysis (Figure 6) revealed the upregulated expression of cellulose synthase genes, including *CesA1*, *CesA3*, *CesA4*, *CesA7*, *CesA8*, and *CesA9*, in *crispr-PagGLR3.3* plants. These cellulose synthases are known to play essential roles in determining cellulose quantity, cell wall quality, and the crystallinity of G-layer

cellulose in TW (Bhandari et al., 2006; Xu et al., 2021). Additionally, prior research has indicated that *FLA* genes are highly expressed in the G-layers of TW fibers (Lafarguette et al., 2004). Therefore, the high expression levels of both *FLA*s and *CesA*s in *crispr-PagGLR3.3* mutants might be associated with the formation of the G-layers. Similarly, the elevated expression of *FLA*s and *CesA*s 10 h after gravistimulation in control plants correlates with the rapid lifting of their stems, presumably due to TW formation. Collectively, these findings demonstrate that reduced Ca^{2+} levels contribute to G-layer formation.

Ca^{2+} induces TW by promoting the accumulation of $O_2^{\cdot-}$

In our recent study, we found that the levels of $O_2^{\cdot-}$ were significantly elevated in the cambium zone of TW compared to opposite wood (OW) after 12 h of gravistimulation. Statistically significant differences became apparent at 24 h. The increased $O_2^{\cdot-}$ levels induced the accumulation of IAA on the upper side of the stems 24 h post-gravistimulation, with a pronounced disparity relative to the lower side emerging at 48 h (Huang et al., 2024). The elevated $O_2^{\cdot-}$ levels activate downstream IAA signaling pathways, thereby stimulating cambium cell proliferation and initiating the TW formation process (Huang et al., 2024). The variations in Ca^{2+} levels between the upper and lower sides of PPCs were observed within 2 h following gravity-induced stimulation, suggesting that Ca^{2+} may function as an initial signal for TW formation. PagGLR3.3 is mainly expressed within the phloem, including PPCs (An et al., 2024), whereas gravity-sensing cells containing starch-filled amyloplasts are predominantly located in the endodermis and phloem (Gerttula et al., 2015). This distribution suggests that PPCs with high Ca^{2+} levels may function as local signaling intermediaries, relaying signals from endodermal and phloem cells to cambium/wood-forming cells. Although an asymmetric Ca^{2+} distribution in PPCs was observed on both the upper and lower sides of stems under gravistimulation in both control and *crispr-PagGLR3.3* lines, the degree of asymmetry was more pronounced in the control group compared to the *crispr-PagGLR3.3* plants. The prolonged time and the reduced magnitude observed in establishing this pattern in *crispr-PagGLR3.3* mutants may account for the delayed primary and secondary bending responses. Notably, the difference in Ca^{2+} levels between the upper and lower sides of the stem diminished significantly within a few hours, indicating that early Ca^{2+} fluctuations induced by gravistimulation function as an initial signaling mechanism for TW induction.

The inactivation of calcium signals caused by Ca^{2+} channel disruption can activate intracellular downstream physiological and biochemical responses (Dodd et al., 2010; Tian et al., 2020; Lee et al., 2021). Protein kinases play crucial roles in these signal transduction pathways. Based on transcriptomic data, we identified that several genes encoding CRKs, CBL4, CDPKs, and other protein kinases were significantly upregulated in the *PagGLR3.3* mutant. These kinases are known to activate auxin signaling (Ludwig et al., 2004; Tripathi et al., 2009; Rigó et al., 2013; Kumar Meena et al., 2019; Tan et al., 2021) and regulate cell wall biosynthesis (Benjamins et al., 2003; Li et al., 2017). Therefore, we speculate that the reduction in $[Ca^{2+}]_{cyt}$ in *crispr-PagGLR3.3* plants, likely caused by ion channel disruption, activates relevant protein kinases, thereby initiating a downstream phosphorylation cascade to sense changes in Ca^{2+} concentration. The expression of these protein kinases was rapidly altered in control plants but showed delayed kinetics in *crispr-PagGLR3.3* plants under gravistimulation, which may account for the temporal differences observed in shoot tip bending and stem lifting. These findings indicate that the asymmetric distribution of Ca^{2+} contributes to the formation of TW and OW, mediated by GLR-dependent Ca^{2+} influx during the early stages of gravitropic responses. Previous studies have reported that CDPKs stimulate ROS-dependent signaling by activating RBOH through direct phosphorylation (Yu et al., 2018; Li et al., 2024). To investigate whether initial changes in Ca^{2+} concentration trigger $O_2^{\cdot-}$ accumulation, we stained the stems of $LaCl_3$-treated 84 K plants and *crispr-PagGLR3.3* plants with NBT and observed significantly higher $O_2^{\cdot-}$ accumulation in their cambium zones compared to control plants (Figure 7). Transcriptomic data revealed elevated expression levels of genes such as RBOHC and CICDH in *crispr-PagGLR3.3* plants, which are known to contribute to ROS production (Mhamdi et al., 2010; Zhang et al., 2022; Pasternak et al., 2023). Based on these observations, we propose that reduced Ca^{2+} levels promote $O_2^{\cdot-}$ accumulation in the cambium zone. Huang et al. (2024) showed that elevated $O_2^{\cdot-}$ accumulation in the upper stem, occurring 12 h after gravistimulation, plays a critical role in TW formation. In the present study, changes in Ca^{2+} levels were detected as early as 2 h post-gravistimulation. These results support a model in which early Ca^{2+} fluctuations in response to gravistimulation initiate downstream ROS production, ultimately contributing to TW formation.

In summary, we investigated the role of Ca^{2+} in modulating TW formation during the early gravitational response by contrasting the differences in Ca^{2+} distribution in PPCs on the upper and lower sides of stems mediated by PagGLR3.3 under gravistimulation. Subsequent transcriptomic analysis validated that reduced Ca^{2+} levels induce the expression of genes associated with gravity perception, ROS, and TW formation. This study deepens our understanding of the Ca^{2+}-mediated signal transduction pathway regulating wood formation and offers potential avenues for manipulating wood properties, such as vessel density and cellulose content.

MATERIALS AND METHODS

Plant materials and growth conditions

The poplar trees used in this study were hybrid white poplar (*P. alba* × *P. glandulosa*) clone 84 K and two homologous *GLR3.3* gene (*GLR3.3a* and *GLR3.3b*) knockout transgenic *crispr-PagGLR3.3* plants that had previously

been obtained (An et al., 2024). We also created *PagGLR3.3a* and *PagGLR3.3b* overexpression plants. The tissue-cultured poplar seedlings were allowed to grow for 1 month after rooting and were then placed in soil in 0.5-L pots with a transparent lid (Super Sprouter) to adjust the ambient humidity for the first 2 weeks. The plants were used for the experiments after they had grown in soil for 1 month. The growth chamber was set to 16 h of white light with 150 μmol m^{-2} s^{-1} irradiation at 24°C and 8 h of darkness at 20°C.

$LaCl_3$ treatments

The calcium channel inhibitor ($LaCl_3$) was prepared at concentrations of 100 mM, 200 mM, and 300 mM and thoroughly mixed with melted lanolin by stirring (Rentel and Knight, 2004; Bjorklund et al., 2007). The mixture was brushed on young stems (third to fifth internodes) and replaced every 3 d. Reverse osmosis (RO) water mixed with melted lanolin served as the control. After the observation of the stem lifting of plants treated with different concentrations of $LaCl_3$, we selected 300 mM $LaCl_3$ concentration for the following experiments. To eliminate the influence of Cl^-, 450 mM $CaCl_2$ and 900 mM KCl were also used to induce gravity in the plants. The experiment was repeated three times.

Calcium antimoniate precipitate and transmission electron microscopy

The samples were prepared for TEM following the method described by An et al. (2014). The sample site was in the middle of the stem between the base and the bent point of the apex (primary bending), and it was the site where the TW was intensively formed in the later stage (secondary bending). The site is indicated by the red arrow in Figure 1A. The upper and lower side tissues from the same site of the stem were peeled and immediately fixed by vacuum infiltration in 2% potassium pyroantimonate, 2.5% (*v*/*v*) glutaraldehyde in 0.2 M potassium phosphate buffer (pH 7.2), with three changes for 15 min each. These tissues were post-fixed overnight in 2% (*w*/*v*) OsO_4, subsequently cleared three times in 0.2 M sodium phosphate buffer (pH 7.2), progressively dehydrated through a graded series of ethanol and acetone solutions, and finally embedded in SPURR (18300-4221, SPI SUPPLIES, West Chester, PA, USA) overnight at 70°C. For visualization by TEM, ultrathin sections (70–90 nm) were stained with methanolic uranyl acetate for 20 min and stained with Reynold's lead citrate for 3 min. Sections were rinsed with double-distilled water. All TEM images were acquired at 100 kV using a TEM 1010 instrument (JEOL, Tokyo, Japan) equipped with an XR-41B AMT digital camera (Advanced Microscopy Techniques, Woburn, MA, USA). The experiment consisted of three biological replicates and was repeated three times. Images of phloem parenchymal cells (PPCs) adjacent to the cambium were randomly selected, and the number of Ca^{2+} points per area (50 × 50 μm) was quantified using ImageJ software.

Fluorescence calcium measurement by an indicator

Ca^{2+} fluorescence was measured using a fluorescence calcium indicator (Fluo-3 AM, ab145254, Abcam, Cambridge, UK). The aforementioned upright or gravity-induced stems were promptly segmented and immediately submerged in 2.5% (*v*/*v*) glutaraldehyde in 0.2 M potassium phosphate buffer (pH 7.2), and sectioned to a thickness of 50 μm using a Leica VT1200S (Wetzlar, Germany) and then immediately transferred to the fluorescence dye for incubation at 37°C for 1 h. The sections were washed with PBS and visualized under an Olympus FV3000 (Tokyo, Japan) confocal microscope (fluorescence intensity at Ex/Em = 490/525 nm). ImageJ software was used to analyze the signal intensity in each rectangular selection box 250 × 50 μm in size between the xylem and phloem fibers. The fluorescence intensity value was analyzed within rectangular selection boxes using the plot profile method (Huang et al., 2024). The experiment was repeated three times.

SEM-EDX analysis

The above stems were also used to measure the Ca^{2+} content by SEM-EDX. 0.5 cm upright or gravity-induced stems were collected and fixed by vacuum infiltration in 2% potassium pyroantimonate and 2.5% (*v*/*v*) glutaraldehyde in 0.2 M potassium phosphate buffer (pH 7.2). To prevent cell surface deformation, tissues that were subjected to cold field emission scanning electron microscope (SEM) (SU8010, Hitachi, Tokyo, Japan) analyses were dehydrated by using drying instruments (TS8606, Fevik, Germany). Energy-dispersive X-ray (EDX) line-scans, accelerating voltages of 15 kV, and a 10 uA beam current were used. K^+ and Ca^{2+} were selected as the target elements. The relative content of ions was expressed as counts per second (cps). The experiment was repeated three times.

Measurement of Ca^{2+} flux

The net fluxes of Ca^{2+} were determined using MNT-NRP-53C10 (Xuyue Company, Beijing, China), a non-invasive technique for measuring the dynamic flow direction and the rate of ions or material surfaces. Ca^{2+} fluxes were measured as previously reported (Zhang et al., 2009; Zheng et al., 2013). In brief, the newly grown adventitious roots were equilibrated in a solution containing 5 mM Ca^{2+} for 30 min, and then transferred to the measuring solution (1.0 mM KCl, 0.5 mM $CaCl_2$, and 0.2 mM MES, pH 5.8). The measurements were performed on five plants at room temperature (24°C–26°C), at least 10 min for each plant. The microelectrode was vibrated in the measuring solution between 5 and 35 mm from the meristem cells' surface along an axis perpendicular to the root. The background was recorded by vibrating the electrode in a measuring solution without roots.

Cell wall composition

The eighth to 12th internodes of 1-month-old control and *crispr-PagGLR3.3* plants in soil were collected for cell wall composition determination. The obtained xylem samples were ground and dried in an oven. Samples were treated with alcohol to obtain insoluble residues, and the lignin content

was measured using the acetyl bromide method (Fukushima and Hatfield, 2001; Moreira-Vilar et al., 2014). The crystalline cellulose content was analyzed by hydrolyzing the residues with Updegraff reagent after treatment with trifluoroacetic acid. After the treated pellets were washed and hydrolyzed with 72% sulfuric acid, the content was quantified using an anthrone assay (Updegraff, 1969; Song et al., 2013). Hemicellulose content was measured using the 3,5-dinitro salicylic acid colorimetric method (M1719A, Michy Biomedical Technology, Suzhou, China). The data from three biological replicates were analyzed.

Plant treatments, stem lift, and microscopy

Graviresponse and stem lift were measured as previously described (Gerttula et al., 2015). After 2 weeks of horizontal gravistimulation, stem lift was measured as the vertical linear distance from the base of the stem to the point at which primary stem (apex) bending occurred initially during gravistimulation. To minimize the effect of slow plant growth on the stem lift measurement, we normalized the vertical distance of the apex to the total stem height as described by Gerttula et al. (2015) and presented the data over time. Stem curvature was measured as the angle between the stem and the horizontal line. A time-lapse camera (T1000 TS, aTLi, Shenzhen, China) was used to record plant performance. Data were obtained from digitized tracings of stems from individual frames of the time-lapse movies. The experiment was repeated three times.

Histochemical and immunolocalization analyses

For G-layer staining, stem cross-sections were immersed in 1% Astra Blue (sc-214558A, Santa Cruz Biotechnology, Dallas, TX, USA) and 5% safranin and then viewed under a microscope (Robards and Purvis, 2009; Gao et al., 2021). The inner layer of a blue-stained cell wall was regarded as a G-layer. The width of TW, as indicated by the blue-stained inner cell wall, was measured, and the number of cell layers with a G-layer was also determined on the basis of more than 10 randomly selected images for analysis.

For cellulose staining, stem cross-sections were washed with PBS and distilled H_2O and then immersed in 0.01% Calcofluor White M2R (Sigma, Louis, MO, USA); for lignin staining, sections were immersed in 2% phloroglucinol/HCl (Gritsch et al., 2015). Stained sections were immediately observed with a light microscope (DM6B, Leica, Wetzlar, Germany). The experiment was repeated three times.

Histological immunolocalizations were performed as previously described (Gerttula et al., 2015). In brief, stem cross-sections were fixed in methanol (80%) at room temperature for 20 min and then washed three times with PBS (1× PBS containing 0.2% Tween 20) for 15 min each time. Sections were then blocked (1× PBS with 5% milk) for 1 h prior to the addition of the primary antibody. The JIM14 antibody (biotin-xx-goat anti-rat IgG, Carbo source services) (#ZW00014) was diluted 1:200 (Gerttula et al., 2015) and the LM5 (ELD007) antibody was diluted 1:100 (Gritsch et al., 2015; Xu et al., 2021), and incubated overnight at 4°C. The monoclonal antibodies of JIM14 and LM5 were obtained from Abmart (Shanghai, China) and Kerafast (CA, USA). Sections were washed three times in 1× PBS and immersed in streptavidin Alexa Fluor-488 at a dilution of 1:400 (Life Technologies, Carlsbad, CA, USA). After 1 h of incubation at room temperature, sections were washed three times in PBS before visualization with a Zeiss LSM880 confocal microscope (Oberkochen, Germany). The experiment was repeated three times.

The $O_2^{\cdot-}$ level was measured by NBT staining. Plant seventh internodes (approximately 5 mm in length) were infiltrated with 1 mg/mL NBT (IN0110, Solarbio, Beijing, China) in the dark for 8 h at 25°C. The internodes were then transferred into 75% ethanol for 8 h and sectioned at a thickness of 50 μm. Samples were observed and photographed using an upright microscope (DM6B, Leica, Wetzlar, Germany). The microscope settings were constant across all the slides throughout the same test. ImageJ software was used to analyze the signal intensity (Schneider et al., 2012) to obtain a series of average OD values across the cambium area following the previous method (Huang et al., 2024). The experiment was repeated three times. In short, to ensure consistent adjustment parameters across different images within the same test, these images were aligned to comparable sizes based on their scale bars and imported into ImageJ software. We used the Analyze-Set Scale function to convert pixels into actual length units. To semi-quantify immunofluorescence intensity (e.g., Ca^{2+}), the cambium zone was selected along its midline using a series of adjacent rectangular boxes. The Analyze-Plot Profile function then generated average gray values (GVs) for each vertical pixel column. For $O_2^{\cdot-}$ analysis, GVs were converted into optical density (OD) values using the Analyze–Calibrate–Uncalibrated OD function, and the same rectangular selection and Plot Profile steps were repeated to obtain the average OD values. The vertical height of the selection boxes was kept constant for all images within a test.

Illumina sequencing and data processing

One-month-old soil 84 K and *crispr-PagGLR3.3#9* poplars were placed horizontally to induce gravistimulation, and the fourth to eighth stem segments (form TW) were harvested immediately and frozen in liquid nitrogen at different time points (0, 2, 4, and 10 h). The upper and lower sides of the samples could not be distinguished at 0 h, and the upper and lower side tissues of the segments as two separate samples were collected at 2, 4, and 10 h. Tissues were scratched from the surface of the bark to the developing xylem, immediately frozen in liquid nitrogen, and stored at −80°C for the isolation of total RNA. Three biological replicates with a total of 42 samples were collected. Total RNA was isolated using the RN38 EASYspin Plus Plant RNA Kit (Aidlab Biotech, Beijing, China), and the quality and purity of RNA samples were determined using a Bioanalyzer 2100 and a Nano LabChip Kit (Agilent, Santa Clara, CA, USA). RNA was then used for sequencing library preparation according to the protocol for the RNA-Seq sample preparation kit (Illumina, San Diego, CA, USA). Paired-end 150-bp sequencing

was performed on the Illumina HiSeq platform. Raw data were filtered with the fastp v.0.20.0 program using default parameters. The clean data were mapped to the *Populus* genome v4.1 (https://phytozome-next.jgi.doe.gov/info/Ptrichocarpa_v4_1) using HISAT2 v2.2.1. The number of reads was calculated using featureCounts v2.0.1, and the DEGs were analyzed using the DESeq. 2 v1.38.3 R package. The plots were produced using the ggplot2 R package. WGCNA was performed using the WGCNA v.1.71 R package.

Gene expression analysis

Expression of target genes was assessed using quantitative real-time PCR (qRT-PCR). Total RNA was isolated using an RN38 EASYspin Plus Plant RNA Kit (Aidlab Biotech, Beijing, China). After quantification, 1 μg of total RNA was reverse-transcribed using Superscript III reverse transcriptase (Invitrogen, Carlsbad, CA, USA). Quantitative reverse transcriptase PCR was then performed on a LightCycler 480 Thermal Cycler (Roche, Basel, Switzerland) using a SYBR Premix Ex TaqTM Kit (TaKaRa, Dalian, China) according to the manufacturer's instructions. All reactions were performed with at least four technical replicates, and the experiment was repeated three times. The *PtrUBQ* gene was used as an internal control gene. The primers for gene expression are summarized in Table S1.

Statistical analysis

The statistical analysis of the number of Ca^{2+} deposits, tension wood phenotypes, and qRT-PCR data was carried out using Student's t-test and is presented as the mean ± *SD*. $^{*}P < 0.05$, $^{**}P < 0.01$.

Data availability statement

The raw data of RNA-seq for poplars under gravistimulation at different times are available in the China National GeneBank DataBase with accession number CNP0004058.

ACKNOWLEDGEMENTS

This study was supported by the National Key Research and Development Program of China "International Cooperation in Science and Technology Innovation between Governments (2019YFE0119100)"; the National Natural Science Foundation of China (NO. 32371902); and the research foundation of Zhejiang A&F University (2018FR013).

CONFLICTS OF INTEREST

The authors declare no conflicts of interest.

AUTHOR CONTRIBUTIONS

M.Z.L. and A.G. designed the experiments. Y.A., M.Q.Q., Y.G., and X.J. performed the experiments. L.C.H., Z.J., X.Q.S., S.T.Z., and S.G. analyzed the data. Y.A. prepared the manuscript. M.Z.L., A.G., S.G., X.H., and J.H.W. helped with manuscript editing. All authors have read and approved the contents of this paper.

Edited by: Legong Li, Capital Normal University, China

Received Jun. 7, 2025; **Accepted** Jan. 2, 2026

REFERENCES

Aldon, D., Mbengue, M., Mazars, C., and Galaud, J.P. (2018). Calcium signalling in plant biotic interactions. Int. J. Mol. Sci. **19:** 665.

An, Y., Geng, Y., Liu, Y., Han, X., Huang, L., Zeng, W., Zhang, J., and Lu, M. (2024). The glutamate receptor gene *GLR3.3*: A bridge of calcium-mediated root development in poplar. Hortic. Plant J. **10:** 1449–1462.

An, Y., Han, X., Tang, S., Xia, X.L., and Yin, W.L. (2014). Poplar GATA transcription factor is capable of regulating chloroplast ultrastructure, photosynthesis, and vegetative growth in under varying nitrogen levels. Plant Cell Tissue Organ Cult. **119:** 313–327.

An, Y., Liu, Y., Liu, Y., Lu, M., Kang, X., Mansfield, S.D., Zeng, W., and Zhang, J. (2021). Opportunities and barriers for biofuel and bioenergy production from poplar. Glob. Change Biol. Bioenergy **13:** 905–913.

Andersson-Gunneras, S., Mellerowicz, E.J., Love, J., Segerman, B., Ohmiya, Y., Coutinho, P.M., Nilsson, P., Henrissat, B., Moritz, T., and Sundberg, B. (2006). Biosynthesis of cellulose-enriched tension wood in *Populus*: Global analysis of transcripts and metabolites identifies biochemical and developmental regulators in secondary wall biosynthesis. Plant J. **45:** 144–165.

Arend, M. (2008). Immunolocalization of (1,4)-beta-galactan in tension wood fibers of poplar. Tree Physiol. **28:** 1263–1267.

Benjamins, R., Ampudia, C.S., Hooykaas, P.J., and Offringa, R. (2003). PINOID-mediated signaling involves calcium-binding proteins. Plant Physiol. **132:** 1623–1630.

Bhandari, S., Fujino, T., Thammanagowda, S., Zhang, D., Xu, F., and Joshi, C.P. (2006). Xylem-specific and tension stress-responsive coexpression of KORRIGAN endoglucanase and three secondary wall-associated cellulose synthase genes in aspen trees. Planta **224:** 828–837.

Bjorklund, S., Antti, H., Uddestrand, I., Moritz, T., and Sundberg, B. (2007). Cross-talk between gibberellin and auxin in development of *Populus* wood: Gibberellin stimulates polar auxin transport and has a common transcriptome with auxin. Plant J. **52:** 499–511.

Björkman, T., and Cleland, R.E. (1991). The role of extracellular free-calcium gradients in gravitropic signalling in maize roots. Planta **185:** 379–384.

Cheng, Y., Zhang, X., Sun, T., Tian, Q., and Zhang, W.H. (2018). Glutamate receptor Homolog3.4 is involved in regulation of seed germination under salt stress in Arabidopsis. Plant Cell Physiol. **59:** 978–988.

Devireddy, A.R., Liscum, E., and Mittler, R. (2020). Phytochrome B is required for systemic stomatal responses and reactive oxygen species signaling during light stress. Plant Physiol. **184:** 1563–1572.

Dodd, A.N., Kudla, J., and Sanders, D. (2010). The language of calcium signaling. Annu. Rev. Plant Biol. **61:** 593–620.

Du, J., Gerttula, S., Li, Z., Zhao, S.T., Liu, Y.L., Liu, Y., Lu, M.Z., and Groover, A.T. (2020). Brassinosteroid regulation of wood formation in poplar. New Phytol. **225:** 1516–1530.

Felten, J., and Sundberg, B. (2013) Biology, chemistry and structure of tension wood. In *Cellular Aspects of Wood Formation. Plant Cell Monographs*. Fromm, J., ed, Volume **20**. (Berlin, Heidelberg: Springer).

Felten, J., Vahala, J., Love, J., Gorzsas, A., Ruggeberg, M., Delhomme, N., Lesniewska, J., Kangasjarvi, J., Hvidsten, T.R., Mellerowicz,

E.J., et al. (2018). Ethylene signaling induces gelatinous layers with typical features of tension wood in hybrid aspen. New Phytol. **218:** 999–1014.

Foyer, C.H., and Hanke, G. (2022). ROS production and signalling in chloroplasts: Cornerstones and evolving concepts. Plant J. **111:** 642–661.

Fromm, J. (2010). Wood formation of trees in relation to potassium and calcium nutrition. Tree Physiol. **30:** 1140–1147.

Fukushima, R.S., and Hatfield, R.D. (2001). Extraction and isolation of lignin for utilization as a standard to determine lignin concentration using the acetyl bromide spectrophotometric method. J. Agric. Food Chem. **49:** 3133–3139.

Gao, J., Jebrane, M., Terziev, N., and Daniel, G. (2021). Enzymatic hydrolysis of the gelatinous layer in tension wood of Salix varieties as a measure of accessible cellulose for biofuels. Biotechnol. Biofuels **14:** 141.

Gerttula, S., Zinkgraf, M., Muday, G.K., Lewis, D.R., Ibatullin, F.M., Brumer, H., Hart, F., Mansfield, S.D., Filkov, V., and Groover, A. (2015). Transcriptional and hormonal regulation of gravitropism of woody stems in *Populus*. Plant Cell **27:** 2800–2813.

Gilroy, S., and Trewavas, A. (2001). Signal processing and transduction in plant cells: The end of the beginning? Nat. Rev. Mol. Cell Biol. **2:** 307–314.

Gorshkova, T., Chernova, T., Mokshina, N., Ageeva, M., and Mikshina, P. (2018). Plant 'muscles': Fibers with a tertiary cell wall. New Phytol. **218:** 66–72.

Gritsch, C., Wan, Y., Mitchell, R.A., Shewry, P.R., Hanley, S.J., and Karp, A. (2015). G-fibre cell wall development in willow stems during tension wood induction. J. Exp. Bot. **66:** 6447–6459.

Groover, A. (2016). Gravitropisms and reaction woods of forest trees—Evolution, functions and mechanisms. New Phytol. **211:** 790–802.

Huang, L.-C., Li, Y.-Y., Lai, J.-X., An, Y., Song, X.-Q., Zhao, S.-T., Zhang, J., and Lu, M.-Z. (2024). Superoxide anions induce tension wood formation by promoting cambium cell activity. Plant Physiol. **197:** kiae672.

Iakimova, E.T., and Woltering, E.J. (2017). Xylogenesis in zinnia (Zinnia elegans) cell cultures: Unravelling the regulatory steps in a complex developmental programmed cell death event. Planta **245:** 681–705.

Jin, Y., Yu, C., Jiang, C., Guo, X., Li, B., Wang, C., Kong, F., Zhang, H., and Wang, H. (2020). *PtiCYP85A3*, a BR C-6 oxidase gene, plays a critical role in Brassinosteroid-mediated tension wood formation in poplar. Front. Plant Sci. **11:** 468.

Kobayashi, H., and Fukuda, H. (1994). Involvement of calmodulin and calmodulin-binding proteins in the differentiation of tracheary elements in Zinnia cells. Planta **194:** 388–394.

Kudla, J., Becker, D., Grill, E., Hedrich, R., Hippler, M., Kummer, U., Parniske, M., Romeis, T., and Schumacher, K. (2018). Advances and current challenges in calcium signaling. New Phytol. **218:** 414–431.

Kumar Meena, M., Kumar Vishwakarma, N., Tripathi, V., and Chattopadhyay, D. (2019). CBL-interacting protein kinase 25 contributes to root meristem development. J. Exp. Bot. **70:** 133–147.

Lafarguette, F., Leple, J.C., Dejardin, A., Laurans, F., Costa, G., Lesage-Descauses, M.C., and Pilate, G. (2004). Poplar genes encoding fasciclin-like arabinogalactan proteins are highly expressed in tension wood. New Phytol. **164:** 107–121.

Lam, H.M., Chiu, J., Hsieh, M.H., Meisel, L., Oliveira, I.C., Shin, M., and Coruzzi, G. (1998). Glutamate-receptor genes in plants. Nature **396:** 125–126.

Lautner, S., and Fromm, J. (2010). Calcium-dependent physiological processes in trees. Plant. Biol. (Stuttg.) **12:** 268–274.

Lautner, S., Ehlting, B., Windeisen, E., Rennenberg, H., Matyssek, R., and Fromm, J. (2007). Calcium nutrition has a significant influence on wood formation in poplar. New Phytol. **173:** 743–752.

Lee, H., Ganguly, A., Baik, S., and Cho, H.T. (2021). Calcium-dependent protein kinase 29 modulates PIN-FORMED polarity and Arabidopsis development via its own phosphorylation code. Plant Cell **33:** 3513–3531.

Li, J., Ishii, T., Yoshioka, M., Hino, Y., Nomoto, M., Tada, Y., Yoshioka, H., Takahashi, H., Yamauchi, T., and Nakazono, M. (2024). CDPK5 and CDPK13 play key roles in acclimation to low oxygen through the control of RBOH-mediated ROS production in rice. Plant Physiol. **197:** kiae293.

Li, K., Yang, F., Zhang, G., Song, S., Li, Y., Ren, D., Miao, Y., and Song, C.P. (2017). AIK1, a mitogen-activated protein kinase, modulates abscisic acid responses through the MKK5-MPK6 kinase cascade. Plant Physiol. **173:** 1391–1408.

Liu, B., Liu, J., Yu, J., Wang, Z., Sun, Y., Li, S., Lin, Y.J., Chiang, V.L., Li, W., and Wang, J.P. (2021). Transcriptional reprogramming of xylem cell wall biosynthesis in tension wood. Plant Physiol. **186:** 250–269.

Love, J., Bjorklund, S., Vahala, J., Hertzberg, M., Kangasjarvi, J., and Sundberg, B. (2009). Ethylene is an endogenous stimulator of cell division in the cambial meristem of *Populus*. Proc. Natl. Acad. Sci. U. S. A. **106:** 5984–5989.

Luan, S. (2009). The CBL–CIPK network in plant calcium signaling. Trends Plant Sci. **14:** 37–42.

Ludwig, A.A., Romeis, T., and Jones, J.D. (2004). CDPK-mediated signalling pathways: Specificity and cross-talk. J. Exp. Bot. **55:** 181–188.

Mellerowicz, E.J., and Gorshkova, T.A. (2012). Tensional stress generation in gelatinous fibres: A review and possible mechanism based on cell-wall structure and composition. J. Exp. Bot. **63:** 551–565.

Meyerhoff, O., Müller, K., Roelfsema, M.R.G., Latz, A., Lacombe, B., Hedrich, R., Dietrich, P., and Becker, D. (2005). *AtGLR3.4*, a glutamate receptor channel-like gene is sensitive to touch and cold. Planta **222:** 418–427.

Mhamdi, A., Mauve, C., Gouia, H., Saindrenan, P., Hodges, M., and Noctor, G. (2010). Cytosolic NADP-dependent isocitrate dehydrogenase contributes to redox homeostasis and the regulation of pathogen responses in Arabidopsis leaves. Plant Cell Environ. **33:** 1112–1123.

Miller, N.D., Durham Brooks, T.L., Assadi, A.H., and Spalding, E.P. (2010). Detection of a gravitropism phenotype in glutamate receptor-like 3.3 mutants of *Arabidopsis thaliana* using machine vision and computation. Genetics **186:** 585–593.

Monshausen, G.B., Miller, N.D., Murphy, A.S., and Gilroy, S. (2011). Dynamics of auxin-dependent Ca^{2+} and pH signaling in root growth revealed by integrating high-resolution imaging with automated computer vision-based analysis. Plant J. **65:** 309–318.

Moreira-Vilar, F.C., Siqueira-Soares Rde, C., Finger-Teixeira, A., de Oliveira, D.M., Ferro, A.P., da Rocha, G.J., Ferrarese Mde, L., dos Santos, W.D., and Ferrarese-Filho, O. (2014). The acetyl bromide method is faster, simpler and presents best recovery of lignin in different herbaceous tissues than Klason and thioglycolic acid methods. PLoS ONE **9:** e110000.

Mousavi, S.A., Chauvin, A., Pascaud, F., Kellenberger, S., and Farmer, E.E. (2013). GLUTAMATE RECEPTOR-LIKE genes mediate leaf-to-leaf wound signalling. Nature **500:** 422–426.

Nguyen, C.T., Kurenda, A., Stolz, S., Chetelat, A., and Farmer, E.E. (2018). Identification of cell populations necessary for leaf-to-leaf electrical signaling in a wounded plant. Proc. Natl. Acad. Sci. U. S. A. **115:** 10178–10183.

Nishikubo, N., Awano, T., Banasiak, A., Bourquin, V., Ibatullin, F., Funada, R., Brumer, H., Teeri, T.T., Hayashi, T., Sundberg, B., et al. (2007). Xyloglucan endo-transglycosylase (XET) functions in gelatinous layers of tension wood fibers in poplar–a glimpse into the mechanism of the balancing act of trees. Plant Cell Physiol. **48:** 843–855.

Pasternak, T., Palme, K., and Perez-Perez, J.M. (2023). Role of reactive oxygen species in the modulation of auxin flux and root development in *Arabidopsis thaliana*. Plant J. **114:** 83–95.

Pilate, G., Dejardin, A., Laurans, F., and Leple, J.C. (2004). Tension wood as a model for functional genomics of wood formation. New Phytol. **164:** 63–72.

Price, M.B., Kong, D., and Okumoto, S. (2013). Inter-subunit interactions between glutamate-like receptors in Arabidopsis. Plant Signal. Behav. **8:** e27034.

Ragauskas, A.J., Williams, C.K., Davison, B.H., Britovsek, G., Cairney, J., Eckert, C.A., Frederick, Jr., W.J., Hallett, J.P., Leak, D.J., Liotta, C.L., et al. (2006). The path forward for biofuels and biomaterials. Science **311:** 484–489.

Ravi, B., Foyer, C.H., and Pandey, G.K. (2023). The integration of reactive oxygen species (ROS) and calcium signalling in abiotic stress responses. Plant Cell Environ. **46:** 1985–2006.

Rentel, M.C., and Knight, M.R. (2004). Oxidative stress-induced calcium signaling in Arabidopsis. Plant Physiol. **135:** 1471–1479.

Richter, D.D., Markewitz, D., Trumbore, S.E., and Wells, C.G. (1999). Rapid accumulation and turnover of soil carbon in a re-establishing forest. Nature **400:** 56–58.

Rigó, G., Ayaydin, F., Tietz, O., Zsigmond, L., Kovacs, H., Pay, A., Salchert, K., Darula, Z., Medzihradszky, K.F., Szabados, L., et al. (2013). Inactivation of plasma membrane-localized CDPK-RELATED KINASE5 decelerates PIN2 exocytosis and root gravitropic response in Arabidopsis. Plant Cell **25:** 1592–1608.

Robards, A.W., and Purvis, M.J. (2009). Chlorazol black E as a stain for tension wood. Stain Technol. **39:** 309–315.

Roberts, A.W., and Haigler, C.H. (1990). Tracheary-element differentiation in suspension-cultured cells of Zinnia requires uptake of extracellular Ca^{2+}: Experiments with calcium-channel blockers and calmodulin inhibitors. Planta **180:** 502–509.

Schneider, C.A., Rasband, W.S., and Eliceiri, K.W. (2012). NIH Image to ImageJ: 25 years of image analysis. Nat. Methods **9:** 671–675.

Seybold, H., Trempel, F., Ranf, S., Scheel, D., Romeis, T., and Lee, J. (2014). Ca^{2+} signalling in plant immune response: From pattern recognition receptors to Ca^{2+} decoding mechanisms. New Phytol. **204:** 782–790.

Shao, Q., Gao, Q., Lhamo, D., Zhang, H., and Luan, S. (2020). Two glutamate- and pH-regulated Ca^{2+} channels are required for systemic wound signaling in Arabidopsis. Sci. Signal. **13:** eaba1453.

Somerville, C. (2006). Cellulose synthesis in higher plants. Annu. Rev. Cell Dev. Biol. **22:** 53–78.

Song, X.Q., Liu, L.F., Jiang, Y.J., Zhang, B.C., Gao, Y.P., Liu, X.L., Lin, Q.S., Ling, H.Q., and Zhou, Y.H. (2013). Disruption of secondary wall cellulose biosynthesis alters cadmium translocation and tolerance in rice plants. Mol. Plant **6:** 768–780.

Takahashi, F., and Shinozaki, K. (2019). Long-distance signaling in plant stress response. Curr. Opin. Plant Biol. **47:** 106–111.

Tan, S., Luschnig, C., and Friml, J. (2021). Pho-view of auxin: Reversible protein phosphorylation in auxin biosynthesis, transport and signaling. Mol. Plant **14:** 151–165.

Tian, W., Wang, C., Gao, Q., Li, L., and Luan, S. (2020). Calcium spikes, waves and oscillations in plant development and biotic interactions. Nat Plants **6:** 750–759.

Toyota, M., Spencer, D., Sawai-Toyota, S., Jiaqi, W., Zhang, T., Koo, A.J., Howe, G.A., and Gilroy, S. (2018). Glutamate triggers long-distance, calcium-based plant defense signaling. Science **361:** 1112–1115.

Tripathi, V., Parasuraman, B., Laxmi, A., and Chattopadhyay, D. (2009). CIPK6, a CBL-interacting protein kinase is required for development and salt tolerance in plants. Plant J. **58:** 778–790.

Updegraff, D.M. (1969). Semimicro determination of cellulose in biological materials. Anal. Biochem. **32:** 420–424.

Vahala, J., Felten, J., Love, J., Gorzsas, A., Gerber, L., Lamminmaki, A., Kangasjarvi, J., and Sundberg, B. (2013). A genome-wide screen for ethylene-induced ethylene response factors (ERFs) in hybrid aspen stem identifies ERF genes that modify stem growth and wood properties. New Phytol. **200:** 511–522.

Wang, H., Jin, Y., Wang, C., Li, B., Jiang, C., Sun, Z., Zhang, Z., Kong, F., and Zhang, H. (2017). Fasciclin-like arabinogalactan proteins, PtFLAs, play important roles in GA-mediated tension wood formation in *Populus*. Sci. Rep. **7:** 6182.

Wilkins, K.A., Matthus, E., Swarbreck, S.M., and Davies, J.M. (2016). Calcium-Mediated Abiotic Stress Signaling in Roots. Front. Plant Sci. **7:** 1296.

Wu, L., Joshi, C.P., and Chiang, V.L. (2000). A xylem-specific cellulose synthase gene from aspen (*Populus tremuloides*) is responsive to mechanical stress. Plant J. **22:** 495–502.

Wudick, M.M., Michard, E., Oliveira Nunes, C., and Feijo, J.A. (2018). Comparing plant and animal glutamate receptors: Common traits but different fates? J. Exp. Bot. **69:** 4151–4163.

Xu, W., Cheng, H., Zhu, S., Cheng, J., Ji, H., Zhang, B., Cao, S., Wang, C., Tong, G., Zhen, C., et al. (2021). Functional understanding of secondary cell wall cellulose synthases in *Populus trichocarpa* via the Cas9/gRNA-induced gene knockouts. New Phytol. **231:** 1478–1495.

Yan, C., Gao, Q., Yang, M., Shao, Q., Xu, X., Zhang, Y., and Luan, S. (2024). Ca(2+)/calmodulin-mediated desensitization of glutamate receptors shapes plant systemic wound signalling and anti-herbivore defence. Nat Plants. **10:** 145–160.

Ye, Z.H. (2002). Vascular tissue differentiation and pattern formation in plants. Annu. Rev. Plant Biol. **53:** 183–202.

Yu, B., Liu, N., Tang, S., Qin, T., and Huang, J. (2022a). Roles of glutamate receptor-like channels (GLRs) in plant growth and response to environmental stimuli. Plants **11:** 3450.

Yu, H., Xiao, A., Dong, R., Fan, Y., Zhang, X., Liu, C., Wang, C., Zhu, H., Duanmu, D., Cao, Y., et al. (2018). Suppression of innate immunity mediated by the CDPK-Rboh complex is required for rhizobial colonization in *Medicago truncatula* nodules. New Phytol. **220:** 425–434.

Yu, J., Zhou, C., Li, D., Li, S., Jimmy Lin, Y.C., Wang, J.P., Chiang, V.L., and Li, W. (2022b). A *PtrLBD39*-mediated transcriptional network regulates tension wood formation in *Populus trichocarpa*. Plant Commun. **3:** 100250.

Zhang, X., Bian, A., Li, T., Ren, L., Li, L., Su, Y., and Zhang, Q. (2022). ROS and calcium oscillations are required for polarized root hair growth. Plant Signal. Behav. **17:** 2106410.

Zhang, Z.Y., Wang, W.J., Pan, L.J., Xu, Y., and Zhang, Z.M. (2009). Measuring Ca^{2+} influxes of TRPC1-dependent Ca^{2+} channels in HL-7702 cells with non-invasive micro-test technique. World J. Gastroenterol. **15:** 4150–4155.

Zhao, R., Liu, Z., Li, Z., Xu, S., and Sheng, X. (2022). Gravity induces asymmetric Ca^{2+} spikes in the root cap in the early stage of gravitropism. Plant Signal. Behav. **17:** 2025325.

Zheng, D., Han, X., An, Y.I., Guo, H., Xia, X., and Yin, W. (2013). The nitrate transporter NRT2.1 functions in the ethylene response to nitrate deficiency in Arabidopsis. Plant Cell Environ. **36:** 1328–1337.

Zinkgraf, M., Gerttula, S., Zhao, S., Filkov, V., and Groover, A. (2018). Transcriptional and temporal response of *Populus* stems to gravi-stimulation. J. Integr. Plant Biol. **60:** 578–590.

SUPPORTING INFORMATION

Additional Supporting Information may be found online in the supporting information tab for this article: http://onlinelibrary.wiley.com/doi/10.1111/jipb.70158/suppinfo

Dataset S1. Total genes of the 42 collected samples

Dataset S2. Summary of expressed genes in modules

Figure S1. Localization of Ca^{2+} in stems of poplar plants under normal growth
Figure S2. Representative EDX line-scans depicting the relative Ca^{2+} concentrations in the vascular tissues on the upper and lower sides of stem subjected to gravistimulation at various time points
Figure S3. Ca^{2+} distribution represented by the fluorescence intensity in the vascular tissues on the upper and lower sides of stem subjected to gravistimulation at various time points
Figure S4. Response of plants to gravistimulation under various treatments
Figure S5. Net Ca^{2+} fluxes in the roots of plants
Figure S6. G-layers observed in phloem fiber cells of *crispr-PagGLR3.3#9* plants
Figure S7. Cross-sections of the seventh internodes of upright plants of *OEPagGLR3.3a* and *OEPagGLR3.3b* stained with safranin and Astra blue
Figure S8. Deposition of cellulose and lignin in the secondary walls of *crispr-PagGLR3.3#9* plants at the seventh internode
Figure S9. Differences in the abundance of arabinogalactan proteins and (1–4)-β-galactan were observed between CK and *crispr-PagGLR3.3#9* plants. The developing G-Layers were immunolocalized with JIM14 and LM5 antibodies
Figure S10. Gravistimulated poplar plants under $LaCl_3$ treatment
Figure S11. Gravistimulation of 180° rotated 84 K plants with preformed TW
Figure S12. Representative EDX line-scans illustrating the relative Ca^{2+} concentrations in the phloem region of 84 K (CK) and *crispr-PagGLR3.3#9* plants during early gravistimulation
Figure S13. Ca^{2+} fluorescence in the phloem parenchymal cells (PPCs) of control (CK) and *crispr-PagGLR3.3#9* plants under gravistimulation over time
Figure S14. Accumulation of Ca^{2+} in the phloem parenchymal cells (PPCs) under gravistimulation with or without $LaCl_3$ treatment
Figure S15. Principal component analysis (PCA) on all 42 samples collected from various tissues of both control and *crispr-PagGLR3.3#9* plants at multiple time points following gravistimulation
Figure S16. Clustering dendrogram of all expressed genes together with assigned module colors
Figure S17. Heatmap analysis on genes differentially expressed between the control and *crispr-PagGLR3.3#9* plants during gravistimulation induction
Movie S1. Time-lapse movie of CK and *crispr-PagGLR3.3#9* poplars undergoing gravitropic bending. Time-lapse images were captured at 15-min intervals
Movie S2. Time-lapse movie of CK and *crispr-PagGLR3.3#9* poplar shoots undergoing gravitropic bending. Time-lapse images were captured at 1-min intervals
Movie S3. Time-lapse movie of CK, *OEPagGLR3.3a*, and *OEPagGLR3.3b* poplar shoots undergoing gravitropic bending. Time-lapse photography was performed every minute
Table S1. Primers used in the expression analysis of differentially expressed genes in control and *crispr-PagGLR3.3* plants